Ectodysplasin signalling deficiency in mouse models of Hypohidrotic Ectodermal Dysplasia leads to middle ear and nasal pathology

HMG Advance Access published July 4, 2016

Ectodysplasin signalling deficiency in mouse models of Hypohidrotic Ectodermal Dysplasia leads to middle ear and nasal pathology

Ali Azar[1], Chiara Piccinelli[2], Helen Brown[3], Denis Headon[1]†, Michael Cheeseman[1]†*

[1]Developmental Biology Division, Roslin Institute and The Royal (Dick) School of Veterinary Studies, University of Edinburgh, EH25 9RG, Scotland, UK, [2]Veterinary Pathology, The Royal (Dick) School of Veterinary Studies, University of Edinburgh, EH25 9RG, Scotland, UK; [3]Genetics and Genomics Division, Roslin Institute and The Royal (Dick) School of Veterinary Studies, University of Edinburgh, EH25 9RG, Scotland, UK.

†co-corresponding authors

*Correspondence. Michael Cheeseman, Developmental Biology Division, Roslin Institute and The Royal (Dick) School of Veterinary Studies, University of Edinburgh, Easter Bush Campus, Midlothian EH25 9RG, Scotland, UK.
Telephone Number 0131 651 9424.
michael.cheeseman@roslin.ed.ac.uk.

Abstract

Hypohidrotic ectodermal dysplasia (HED) results from mutation of the *EDA*, *EDAR* or *EDARADD* genes and is characterized by reduced or absent eccrine sweat glands, hair follicles and teeth, and defective formation of salivary, mammary and craniofacial glands. Mouse models with HED also carry *Eda*, *Edar* or *Edaradd* mutations and have defects that map to the same structures. Patients with HED have ear, nose and throat disease, but this has not been investigated in mice bearing comparable genetic mutations. We report that otitis media, rhinitis and nasopharyngitis occur at high frequency in *Eda* and *Edar* mutant mice and explore the pathogenic mechanisms related to glandular function, microbial and immune parameters in these lines. Nasopharynx auditory tube glands fail to develop in HED mutant mice and the functional implications include loss of lysozyme secretion, reduced mucociliary clearance and overgrowth of nasal commensal bacteria accompanied by neutrophil exudation. Heavy nasopharynx foreign body load and loss

of gland protection alters the auditory tube gating function and the auditory tubes can become pathologically dilated. Accumulation of large foreign bodies particles in the bulla stimulates granuloma formation. Analysis of immune cell populations and myeloid cell function shows no evidence of overt immune deficiency in HED mutant mice. Our findings using HED mutant mice as a model for the human condition support the idea that ear and nose pathology in HED patients arises as a result of nasal and nasopharyngeal gland deficits, reduced mucociliary clearance and impaired auditory tube gating function underlies the pathological sequelae in the bulla.

Introduction

Development of a wide range of exocrine glands, as well as teeth and hair follicles, relies on the action of the EDAR signaling pathway. This pathway, composed of a TNF-like ligand Ectodysplasin (EDA), its transmembrane receptor EDAR, and the intracellular signal transducer EDARADD, is highly evolutionarily conserved [1] and loss of signaling due to mutation of genes encoding any component of this linear pathway leads to impaired tooth, hair and glandular development. In humans this condition is termed hypohidrotic (or anhidrotic) ectodermal dysplasia (HED), characterized by reduced or absent eccrine sweat glands, hair follicles and teeth, and defective formation of salivary, mammary and craniofacial glands. This is most commonly a result of mutation of the *EDA* gene (OMIM 300451), which lies on the X chromosome. Males hemizygous for *EDA* mutation have the same clinical features as those caused by homozygosity for loss of function mutations in the *EDAR* (OMIM 604095) or *EDARADD* (OMIM 606603) genes, while females heterozygous for *EDA* mutation have variable signs of HED features, due to the stochastic patterns of X chromosome inactivation. Mouse models with HED also carry *Eda*, *Edar* or *Edaradd*

loss of function mutations and have defects that map to the same structures as affected in human HED [1]. HED phenotypes in the *Edar* mutant mouse *downless* are rescued by a yeast artificial chromosome with multiple copies containing approximately 200 kb of mouse genomic DNA across the *Edar* locus, integrated into a site unlinked to the endogenous *Edar* gene on mouse chromosome 10 [2]. This transgenic line, $Edar^{Tg951/951}$, has high level *Edar* expression under control of the gene's endogenous regulatory elements and display morphological changes to the hair, teeth and mammary, sebaceous and salivary glands [3,4].

Patients with HED have dry nose with crusting and concretion of nasal secretions, rhinitis and ozena [5-7], rhinosinusitis and infection, otitis media and speech and hearing impairment, and sore throat [8-10]. These clinical phenotypes have been attributed to reduced sinonasal and auditory tube glands, reduced ciliary function and decreased salivary gland function [9]. HED mutant mice have the same structural defects as those in the human condition and can provide a test of this hypothesis and means to further investigate the underlying pathophysiology of ear, nose and throat disease associated with ectodermal dysplasia.

The embryonic development of nasal glands in mice initiates between days 14 and 17 post-conception. These glands are anatomically complex and in *Tabby* hemizygous male ($Eda^{Ta/Y}$) mice, specific nasal glands subsets are reduced in size, or are absent at birth, while adjacent glands are unaffected. Nasopharynx and auditory (Eustachian) tube glands are absent at birth in $Eda^{Ta/Y}$ mice [11]. *Tabby* [11] and *crinkled* (*Edaradd* mutant: MGI Ref ID J:87623) mice have upper respiratory stertor and in *Tabby* mice this has been attributed to hair in the nose [11].

Despite clinical findings of otitis media in human patients with HED, this phenotype has not been reported in mice bearing comparable genetic mutations. In

this work we show that otitis media, as well as rhinitis and nasopharyngitis, is highly penetrant in *Tabby* (*Eda*$^{Ta/Ta}$ and *Eda*$^{Ta/Y}$; hereafter collectively termed *Eda*^{Ta} mice) and *downless* homozygous (*Edar*$^{dlJ/dlJ}$) mice and explore the pathogenic mechanisms related to glandular function and microbial and immune parameters in these lines.

Results

Edar$^{dlJ/dlJ}$ and *Eda*^{Ta} mice lack nasopharynx glands

The nasopharynx duct of the adult mouse is a ~1.2 mm diameter x ~6 mm long tube (Figure 1A, 1B); its rostral region has nasal associated lymphoid tissue. Submucosal glands, with mixed populations of serous and mucous cells, are located dorsal to the auditory tubes and were present in all wild-type FVB mice (n=36), *Edar*$^{dlJ/+}$ (n=45) and *Edar*$^{Tg951/951}$ (n=23) mice examined (Figure 1A, 1E, 1G, 1I). Small nasopharynx submucosal glands are located caudal to the auditory tube opening (Figure 1C) and were present in all n=6 FVB mice and n=6 *Edar*$^{dlJ/+}$ mice examined. Submucosal glands associated with auditory tube (Figure 1K) and caudal nasopharynx (data not shown) are lysozyme positive. Auditory tube glands were absent in *Edar*$^{dlJ/dlJ}$ (n=52) and *Eda*^{Ta} mice (n=37) (Figure 1F, 1H, 1J, 1L), as were the caudal nasopharynx glands in (n=6) *Edar*$^{dlJ/dlJ}$ and (n=6) *Eda*^{Ta} mice (Figure 1D).

Lateral nasal glands located in the lateral walls of the nasal chambers and medial nasal glands located in the mucosa either side of the nasal septum (Figure 2 A-C) are comprised solely of serous cells. Neither the lateral nor the medial nasal glands stain positively for lysozyme (Figure 2E, 2F). Medial nasal glands in FVB and *Edar*$^{dlJ/dlJ}$ mice, like salivary glands [12], stain for cleaved caspase 3 (Figure 2G, 2H) but the nasopharynx glands of *Edar*$^{dlJ/+}$ mice do not stain for cleaved caspase 3 (data not shown).

We used *Edar*$^{Tg951/951}$ mice [2] that have anatomically normal nasal and nasopharyngeal glands and high levels of *Edar* gene expression [3,4] for in situ hybridization studies to enhance detection of *Edar* mRNA transcripts. The positive RNA control probe *PpiB* (data not shown) and *Edar* RNA probe gave punctate signals in the auditory tube submucosal glands, auditory tube epithelium, nasopharynx epithelium, soft palate submucosal glands, basal cells of oral squamous epithelium (Figure 2I-K), nasal epithelium glands and bone marrow cells (data not shown); but signals were not detected in muscle (Figure 2I, 2J). The negative control probe *DapB* did not give hybridization signals (Figure 2L).

Nasal, nasopharynx and bulla pathology is highly prevalent in *Edar*$^{dlJ/dlJ}$ and *Eda*^{Ta} mice

Edar$^{dlJ/dlJ}$ and *Eda*^{Ta} mice have rhinitis, nasopharyngitis and otitis media (Figure 3A) and the prevalence increases significantly to >70% (P<0.001; Fisher's exact tests) between weaning (3 weeks) and adulthood (7-43 weeks) (Figure 3A). No upper respiratory tract or bulla pathology was observed in *Edar*$^{dlJ/+}$, *Edar*$^{Tg951/951}$ and FVB mice.

Nasal and nasopharynx pathology in *Edar*$^{dlJ/dlJ}$ and *Eda*^{Ta} mice

Rhinitis in *Edar*$^{dlJ/dlJ}$ and *Eda*^{Ta} mice is characterised by inflammatory cell infiltration of the epithelium and mucosa of the nasal septum and ethmoid turbinates. The nasal passages (Figure 3C) and nasopharynx (Figure 1D, 1F, 1H, 1L) contain neutrophils mixed with foreign body particles comprising hair shaft fragments and plant-based material from bedding or food. Nasal wash cytology differentials in *Edar*$^{dlJ/dlJ}$ mice (n=7) were 99.5% neutrophils and 0.5% macrophages.

Nasal epithelium cells with intracytoplasmic hyaline droplets [13] can show cytoplasmic blebbing (Figure 3E, 3F) and the number of affected cells was

significantly increased in *Edar*$^{dlJ/dlJ}$ and *Eda*^{Ta} mice compared to *Edar*$^{dlJ/+}$ and FVB mice at 3 and 12 weeks-of-age (Figure 3B). However this change can be extensive in FVB and *Edar*$^{Tg951/951}$ at 36-47 weeks-of-age without being associated with nasal pathology (data not shown).

The nasopharynx duct in *Edar*$^{dlJ/dlJ}$ and *Eda*^{Ta} mice contains exudate and foreign body particles (Figure 1D, 1F, 1H, 1L). In wild-type FVB mice the dorsal nasopharynx is covered by a ciliated epithelium with goblet cells but in *Edar*$^{dlJ/dlJ}$ and *Eda*^{Ta} mice this undergoes squamous metaplasia and the submucosa is infiltrated by lymphocytes and plasma cells (Figures 3G-J; Figure 8E, 8F) and squamous metaplasia can extend into the proximal auditory tube (Figure 1J). In *Eda*^{Ta} mice there were reduced numbers of Alcian Blue goblet cells (Figure 1I and 1J) (27-weeks-old *Eda*^{Ta}, median 0, 95% CI, 0-4, n=12 auditory tubes versus 37-weeks-old FVB, median 42, 95% CI, 21-64, n=4 auditory tubes; *P*=0.0005 Mann Whitney test) and lysozyme positive secretory cells (Figure 1K and 1L) in the proximal auditory tube compared with FVB mice.

Bulla pathology in *Edar*$^{dlJ/dlJ}$ and *Eda*^{Ta} mice

Adult *Edar*$^{dlJ/+}$, *Edar*$^{Tg951/951}$ and FVB mice have healthy air filled bullae lined by a thin mucosa (Figure 4A, 4B). Grossly visible bulla fluids were evident in 55% of *Edar*$^{dlJ/dlJ}$ (32/58) and 50% (28/56) of *Eda*^{Ta} mice; 74% and 91% of the *Edar*$^{dlJ/dlJ}$ and *Eda*^{Ta} mice respectively had microscopic inflammation of the bulla (Figure 3A, 4C-E, 4G-J). Bulla fluid cytology differentials in (n=5) *Edar*$^{dlJ/dlJ}$ mice were 90.5% neutrophils and 9.0 % macrophages. In contrast to the nasopharynx and auditory tubes where goblet cells are effaced by squamous metaplasia, the intact bulla respiratory epithelium adjacent to auditory tube entrance can have goblet cell hyperplasia (Figure 4B, 4D), elsewhere the submucosa was thickened and infiltrated with inflammatory

cells (Figures 4J). The bulla epithelium and foamy macrophages stain positively for the hypoxia marker pimonidazole (Figures 4E, 4F). Foreign body particles were mixed with bulla exudate (Figure 4J) or associated with organized vascular granulomas. Granulomas were found in the inflamed bullae of 13% and 25% of *Edar*$^{dlJ/dlJ}$ and *Eda*^{Ta} mice respectively, and those illustrated in (Figure 4G, 4I) were located in the caudal bulla.

Loss of auditory tube glands alters tube gating function

Foreign body particles naturally accumulate within the bullae of mice with otitis media and their size is an indicator of auditory tube gating function. The otitis media mutant *Junbo* [14-17] has auditory tube glands (Figure 5C) and provides an out-group comparison for HED mutant mice that lack glands. All n=15 13-45 weeks-old *Junbo* mice examined had bilateral otitis media but there was no evidence of exudate in the nasal passages nor of mucosal inflammation or squamous epithelial change in the nasopharynx (Figure 5A, 5B). We found the median size of foreign body particles in the bullae was significantly larger (P<0.0001) in *Edar*$^{dlJ/dlJ}$ (n=11, 7-17 weeks-old) and *Eda*^{Ta} (n=10, 13-30 weeks-old) mice than it was in *Junbo* mice (n=9, 13-45 weeks-old) (Figure 5F).

The auditory tube lumen appeared enlarged in *Eda*^{Ta} mice particularly when it contained intraluminal foreign body and exudate (Figure 5C, 5D). However, when the tube lumen areas were quantified in step sections, only the auditory tubes in *Eda*^{Ta} mice (n=6) but not *Edar*$^{dlJ/dlJ}$ (n=6) mice were significantly enlarged (P<0.0001) compared to *Junbo* (n=5) or *Edar*$^{dlJ/+}$ (n=6) mice (Figure 5E).

Nasal bacterial infection and inflammatory response in *Edar*$^{dlJ/dlJ}$ and *Eda*^{Ta} mice

To explore the functional implication of nasopharynx gland loss on nasal commensal bacteria populations we cultured the nasal washes. Mice in our specific pathogen free

(SPF) facility are housed in individually ventilated cages to maintain a microbiological barrier between colonies. *Eda*^{Ta}, *Edar*$^{dlJ/dlJ}$, *Edar*$^{dlJ/+}$, and FVB colonies had nasal commensals such as *Gemella* like sp., *Enterococcus* sp., *E. coli*, DNAase negative *Staphylococcus* sp., and *Staphylococcus aureus*, while the SPF *Junbo* colony that originated in a different SPF animal facility had additional nasal commensals such as *Proteus mirabilis*, *Moraxella* sp. and an unidentified Gram-positive bacillus (Table S1).

Nasal washes of *Edar*$^{dlJ/dlJ}$ and *Eda*^{Ta} mice had significantly higher leukocyte numbers (median 7,950 leukocytes, 95% CI, 4,140-13,193, n=34, versus median 0 leukocytes, 95% CI, 0-33, n=28; $P<0.0001$; Mann Whitney test) (Figure 6A) and total bacterial loads (median $10^{4.1}$ CFU, 95% CI, $10^{4.3}$-$10^{5.9}$, n=19 versus median $10^{1.9}$ CFU, 95% CI, $10^{1.3}$-$10^{2.6}$, n=18; $P<0.0001$) compared to *Edar*$^{dlJ/+}$ and FVB mice (Figure 6B). The species of nasal bacteria found in *Edar*$^{dlJ/dlJ}$ and *Eda*^{Ta} mice are significantly different ($P=0.0003$, Fisher's exact test); in *Eda*^{Ta} mice the principal nasal commensal/pathogen was *Staphylococcus aureus* and the total bacterial load was $10^{4.7}$ CFU (median, 95% CI, $10^{3.9}$-$10^{6.3}$, n=10). In *Edar*$^{dlJ/dlJ}$ mice the principal nasal pathogen was *E. coli* and the total bacterial load was $10^{4.1}$ CFU (95% CI, $10^{3.1}$-$10^{6.2}$, n=9). *Edar*$^{dlJ/+}$ and FVB mice had low titres of nasal commensals (in the range of 10^{1}-10^{3} CFU) and no species predominated (see Table S1 for full list of bacterial species and titres). In *Eda*^{Ta} mice cocci colonies were observed associated with foreign body material (Figure 6C).

Junbo mice had the greatest range of nasal bacterial species (Table S1), but the median total bacterial load $10^{2.0}$ CFU (95% CI, $10^{1.5}$-$10^{2.8}$, n=7; $P=0.0005$) and median nasal leukocyte number 132 (95% CI, 0-994, n=7; $P<0.0001$) were significantly lower than those in HED mutants.

Bulla bacterial infection in *Edar*$^{dlJ/dlJ}$, *Eda*^{Ta} and *Junbo* mice

All FVB (n=24) and *Edar*$^{dlJ/+}$ (n=12) bullae sampled were healthy and air-filled and their PBS rinses were culture negative (Figure 6D) and had very few or no leukocytes. A significantly greater proportion of *Junbo* bullae contained fluid (14/14) compared to *Edar*$^{dlJ/dlJ}$ (10/18; *P*=0.0044; Fisher's exact test), and 6/20 *Eda*^{Ta} mice (6/20; *P*<0.0001, Fisher's exact test). High *E. coli* titres of $10^{6.2}$ CFU were isolated from 9/18 *Edar*$^{dlJ/dlJ}$ bullae (median, 95% CI, $10^{3.1}$-$10^{6.2}$) (Figure 6D) and there was a significant positive association between bulla and nasal titres (Spearman rank correlation coefficient R=0.93, *P*=0.0003). Large numbers of intracellular Gram-negative bacilli were observed in foamy macrophages with lipid bodies (Figures 6E-G). Low titres $10^{1.8}$ CFU (median, 95% CI, $10^{1.3}$-$10^{2.1}$) of individual bacteria were found in 3/20 *Eda*^{Ta} bullae, and intermediate titres $10^{3.1}$ CFU (median, 95% CI, $10^{1.5}$-$10^{3.3}$) of single or mixed bacteria were found in 8/14 *Junbo* bullae (Figure 6D; Table S1). There was no association between total bacteria load in the nose and bulla (Spearman rank correlation coefficient R=-0.05, *P*=0.9) in *Junbo* mice.

Immune cell populations and myeloid cell function are comparable in *Edar*$^{dlJ/+}$, *Edar*$^{dlJ/dlJ}$ and *Eda*^{Ta} mice

Edar and *Eda* genes are expressed in neutrophils, macrophages, T cells and B cells (http://www.immgen.org) so we investigated whether this led to alterations in leukocyte populations or myeloid cell function that might predispose to inflammatory disease. The spleens of *Edar*$^{dlJ/dlJ}$ mice had a significantly higher percentage of neutrophils (34.2% versus 19.7%, *P*=0.015; Mann Whitney test) and marginally lower T cells (32.0% versus 28.2%, *P*=0.041) compared to *Edar*$^{dlJ/+}$ littermate controls. All

other myeloid and lymphocyte sub-populations in spleen, peripheral blood, bone marrow and peritoneum were not significantly different (Table S2).

The percentage of phagocytically active peritoneal macrophages was not significantly different in Eda^{Ta}, $Edar^{dlJ/dlJ}$ or $Edar^{dlJ/+}$ mice (Figure 7A, 7B, 7J). $Edar^{dlJ/dlJ}$ and Eda^{Ta} bulla leukocytes are predominantly neutrophils with ~2% macrophages and a high percentage of neutrophils were necrotic or apoptotic (Figure 7C, 7D). Viable bulla neutrophils, macrophages and foamy macrophage were phagocytically active (Figure 7E-J) but the percentage of phagocytically active leukocytes was higher (P<0.001) in Eda^{Ta} mice (Figure 7J).

Pathological sequelae to nasal/nasopharyngeal disease

Patients with HED are reported to have sore throat and acute pharyngo-laryngitis and are predisposed to pulmonary infections [8,9] and so we assessed larynx and lung pathology in HED mice to determine whether they display pathologies in common with the human condition. Eda^{Ta} mice lack submucosal glands associated with the soft palate, larynx and trachea [8, 18] (Figure 8A-H) and the larynx and tracheal glands are lysozyme positive (data not shown). In a histological survey of eight Eda^{Ta}, one $Edar^{dlJ/dlJ}$, two $Edar^{dlJ+}$ and four FVB mice, one Eda^{Ta} mouse had neutrophil leukocyte inflammation of larynx and three had laryngeal lymphoid follicles, but these changes were not observed in the $Edar^{dlJ+}$ and FVB mice (Figure 8A-D). One of the possible sequelae of nasal/nasopharyngeal disease is inhalation of material into the lung but this was uncommon in 12 clinically normal HED mice. One (of six) 27-week-old Eda^{Ta} mice had two solitary foci of bronchiolitis associated with inhaled fragments of hair; and six 13-week-old $Edar^{dlJ/dlJ}$ mice had unremarkable lungs. In rodents, increased resistance to nasopharynx airflow can result in swallowing of air

into the stomach and intestines (aerophagia) [19] and over a two year period we observed eight instances of clinical abdominal bloating in our HED colony mice; seven of eight cases were in adult mice >7-weeks-old; three in Eda^{Ta} males at 3-, 8- and 18-weeks of age respectively, and five cases in 12-15 week-old male and female $Edar^{dlJ/dlJ}$ mice. Post mortem examination revealed a gas filled stomach, small intestine and caecum (Figure 8I). Histopathology of one Eda^{Ta} male revealed a distended empty stomach and GI tract was lined by healthy mucosa (Figure 8J, 8K). The prevalence of aerophagia was low in mice in adult HED mice >7-weeks of age (5/133 $Edar^{dlJ/dlJ}$ and 2/139 Eda^{Ta} mice) and was not significantly different between these strains (P=0.273; Fisher's exact test). Aerophagia has not been observed in $Edar^{dlJ+}$ sibling mice.

Discussion

We report that, in common with human patients with ectodermal dysplasia, HED mutant mice (Eda^{Ta} and $Edar^{dlJ/dlJ}$) have chronic rhinitis and otitis media and these models provide a number of novel insights into the pathogenesis of ear, nose and throat disease. The hypothesis that ear, nose and throat pathology in HED patients arises from impaired mucociliary function associated with hypoplasia/aplasia of glands lining the sinonasal tract and auditory tube [9] is supported, and can now be refined, placing particular importance on the role nasopharyngeal glands and their products.

Embryological studies show that the loss of EDAR signalling in Eda^{Ta} mice leads to the reduction/deletion of medial and lateral nasal gland subsets, deletion of submucosal glands associated with the auditory tube and nasopharynx, but the largest lateral nasal glands, the Steno's glands, are normal [11]. The auditory tube submucosal glands increase in size and start to express lysozyme and lactoferrin on

post-natal day 3 (P3) [20,21]. There are two mouse lysozyme genes; lysozyme M is expressed in macrophages, bone marrow and lung, whereas lysozyme P is expressed in paneth cells and predominates the small intestine [22]. Lysozyme P is expressed in adult auditory tube glands in lysozyme M deficient mice [23] and in this work we show the medial nasal glands and lateral nasal glands do not express lysozyme. Auditory tube secretory epithelial cells also express lysozyme [20,21], but secretory cells may be lost through secondary squamous metaplasia of the auditory tube epithelium in HED mice

Patients with HED are reported to have dry nose and crusting secretions [8,9]. In the mouse model, EDAR signalling effects on the development of nasal gland subsets, as well as lacrimal gland function [24], may compromise nasal homeostasis; the lacrimal gland defects having an influence through reduced tear production and consequent nasal humidification. Adult nasal glands express the *Edar* gene and the loss of EDA signals may also alter nasal gland physiology in HED mice and add to nasal drying. The use of two markers, cleaved caspase 3 and lysozyme, reveals distinct patterns of nasal and nasopharynx submucosal gland expression, implying that nasal glands can not fully compensate for the deletion of nasopharynx glands. It will be a considerable challenge to tease apart the extent nasal gland redundancy and functional reserve.

The accumulation of exudate and foreign body particles in the nasal passages and nasopharynx duct is direct evidence of impaired mucociliary clearance in HED mutant mice. Mucociliary clearance from the nose to the larynx depends on cilia action and mucus viscosity [25] and is achieved by cilia transporting an aqueous periciliary layer and overlying mucus. Lysozyme promotes cilia function [26] so loss of glandular lysozyme may impair cilia function; furthermore ciliated cells are

replaced by squamous epithelium in the inflamed nasopharynx, both contributing to reduced mucociliary clearance. The impact of hyaline droplet change is less clear. Hyaline droplets are a histological feature of rodent nasal respiratory and olfactory epithelium [13] and have no direct counterpart in human nasal pathology. They are a non-specific change associated with ageing and with chronic exposure to inhaled respiratory toxicants [13]. The origin and function of the protein within intracytoplasmic hyaline droplets is currently unknown [27]. Hyaline droplets are nevertheless a useful early marker of upper respiratory tract disease in HED mice. The *Edar* gene is expressed in respiratory epithelium of the trachea [18]. By using the transgenic overexpressing $Edar^{Tg951/951}$ mouse to enhance detection of *Edar* mRNA we found the *Edar* expression in respiratory epithelium of nasal passages, as well as nasopharynx and auditory tubes and submucosal glands. Therefore hyaline droplet change may be a direct result of loss of EDAR signalling on epithelial cells and/or secondary to loss of glandular protection. We note that FVB and $Edar^{Tg951/951}$ mice have normal mucociliary clearance but have age-related hyaline droplet degeneration. This implies that the overall effect of hyaline droplet change on mucociliary clearance via cilia motility, or on mucus composition/viscosity via cytoplasmic blebbing, is likely to be limited.

This work shows two distinct roles of auditory tube submucosal glands in nasopharynx and bulla defence. HED mice have reduced mucociliary clearance and the loss of glandular secretions, such as lysozyme and mucus, creating a niche for the proliferation of endemic nasal bacteria; and secondly, the loss of glands alters auditory tube gating function.

The *Junbo* otitis media mutant, which has auditory tube glands, serves as out-group comparison for HED mice. All the *Junbo* mice examined had bilateral otitis

media and ~60% of bullae had culturable bacteria. However *Junbo* mice did not have significant nasal disease, and the numbers of nasal commensal bacteria were comparable to FVB and $Edar^{dlJ/+}$ mice without otitis media, suggesting that auditory tube glands play a role in regulation of commensal populations. $Edar^{dlJ/dlJ}$ and Eda^{Ta} mice are phenocopies with respect cranial gland deficits and upper respiratory tract pathology, but show differences in nasal commensal pathogens that probably stem from the microbiological barrier between the two colonies in our animal facility.

The principal nasal pathogen in Eda^{Ta} mice was *Staphylococcus aureus,* but in $Edar^{dlJ/dlJ}$ mice it was *E. coli.* The spread of nasal bacteria into the bulla is a potential inflammatory stimulus for otitis media and in $Edar^{dlJ/dlJ}$ mice the *E. coli* titres in the nose and bullae are positively correlated. The *E. coli* strains involved have adopted an intracellular lifestyle in bulla foamy macrophages and lipid bodies may aid their intracellular survival [28]. The inflamed bulla of HED mice, and *Junbo* mice [15-17], is hypoxic and under hypoxic conditions bactericidal activity of macrophages against *E. coli* and *Staphylococcus aureus* is inhibited [29]. In Eda^{Ta} mice, *Staphylococcus aureus* bulla infection was uncommon implying that this bacterium does not readily ascend the auditory tube and/or is more effectively cleared from the bulla.

Dogs with X-linked HED have a higher incidence of respiratory disease but this is not attributable to an overt deficiency in the adaptive or innate immune systems [30]. Nevertheless, we considered whether HED mutant mice might have an immunological deficit, particularly if it affected neutrophil and macrophage populations or function in the nose and bulla. We found that myeloid cells and lymphocyte sub-populations in peripheral blood, bone marrow and peritoneum of $Edar^{dlJ/dlJ}$ and $Edar^{dlJ/+}$ mice were broadly similar. Neutrophils were elevated in $Edar^{dlJ/dlJ}$ spleens but there was no accompanying leucocytosis to suggest a marked

systemic inflammatory response to nasal and bulla disease. There was no significant difference between phagocytic activity of *Edar*$^{dlJ/dlJ}$, *Edar*$^{dlJ/+}$ or *Eda*^{Ta} peritoneal macrophages.

The bulla fluid inflammatory cells are predominately neutrophils, comprising viable, apoptotic and necrotic neutrophils, and a smaller population of macrophages. The percentage of viable bulla neutrophils and macrophages that were phagocytically active was significantly lower in *Edar*$^{dlJ/dlJ}$ compared to *Eda*^{Ta} mice. This is unlikely to have to genetic basis because the phagocytic activity of *Edar*$^{dlJ/dlJ}$ and *Eda*^{Ta} peritoneal macrophages was comparable. Given the high *E. coli* infection rates in *Edar*$^{dlJ/dlJ}$ bullae, one explanation is that the leukocytes were already actively engaged bacterial phagocytosis in these animals and that this impaired the cells' performance in the ex vivo assay.

A second mechanism of otitis media HED mutant mice is that gland loss alters auditory tube gating function. In comparison to *Junbo* mice, HED mice accumulate larger particles in the bulla yet have a lower prevalence of bulla fluids. We interpret this as a reduced capacity to exclude larger particles, possibly exacerbated by failure to clear larger particles along with inflammatory bulla fluids. In *Df1*/+ and *Tbx*$^{+/-}$ mouse models of 22q11.2 deletion syndrome, otitis media is associated with developmental hypoplasia of the levator veli palatini muscles that control auditory tube clearance [31]. In the RPL38 deficient Tail-short (Ts) mouse auditory tube enlargement, bulla inflammation, cholesterol crystal accumulation and ectopic ossification occur concurrently and auditory tube dysplasia may contribute to the chronicity of otitis media in this mouse strain [32]. The absence of auditory tube dilation in *Junbo* mice may relate to bulla infection/inflammation inducing auditory tube gland enlargement via hypertrophy of the mucous cell population. In the rat,

bulla infection causes gland enlargement, narrowing of the auditory tubes and altered mucus composition/viscosity that impairs bulla clearance and prolongs otitis media [33]. The accumulation of significantly larger foreign body particles in bullae of HED mutant mice compared to *Junbo* mice is associated with a heavy foreign body load in the nasopharynx, coupled with a loss of glandular mucus and reduced capacity for particle trapping. It is noteworthy that, unlike Eda^{Ta} mice, the auditory tubes of $Edar^{dlJ/dlJ}$ of mice sampled in this study were not enlarged. This indicates that tube enlargement is not a primary event in bulla pathology in HED mice but is a secondary pathological change. The space-occupying effect of the submucosal glands on the medial margin of the auditory tube may be a factor in maintaining tube shape, and gland absence in HED mice may contribute to pathological tube dilation. The importance of auditory tube glands in maintaining a barrier to entry of large particles is underlined by the formation foreign body granulomas in the bullae of HED mice. To our knowledge this represents a unique otitis media phenotype not seen in other published mouse models. One of the pathological sequelae in HED mice was sporadic clinical aerophagia. In adult rats, increased resistance to airflow by experimental obstruction of the nasal passages causes aerophagia [19] and spontaneous nasal/nasopharynx disease in HED mice may have the same effect.

In summary, these mouse strains model not only the genetic, signalling and developmental structural defects of human HED, but also many of the secondary pathological effects resulting from reduced mucociliary clearance and innate immune system function with respect to glandular secretions. The novel insights gained from studying mouse are that the submucosal glands of the nasopharynx have a critical regional role in the protection the auditory tube and bulla. Respiratory epithelium [34] and auditory tube epithelial secretory cells [21] produce a range of innate immune

antimicrobials such as lysozyme, lactoferrin, mucins, ß-defensins, but when mucociliary clearance is impaired, loss of auditory tube gland secretions such as lysozyme compromise control of nasal commensal bacteria. Secondly, gland loss in HED mice may contribute to pathological tube dilation and this is not compensated for by the action of auditory tube muscles that control bulla clearance [31].

HED mice develop nasal and bulla disease spontaneously within the cage environment through exposure to environmental bacteria, hair and dust. This makes HED mice a reproducible and robust animal model, but we note that certain aspects of the mouse disease phenotype differ from those in humans. HED patients are reported to have sinusitis and sore throat [8,9] but in HED mice inflammation of the larynx was minor pathological feature and the sinuses are not affected. Hyaline droplets are a convenient biomarker for respiratory cell injury/senescence in rodent models but this change is not directly relevant to clinical HED. Obstruction to nasal airflow in HED patients is related craniofacial features such as a broad nose, depressed nasal bridge and wider nasal fossae, nasal dryness and crusting [9]. In mice, which are obligate nose breathers, obstruction to nasal airflows may be the cause of sporadic aerophagia. In spite of these species differences, the findings in mouse models suggest there may be may be important clinical correlates to discover in HED patients, such as altered auditory tube patency/function, as well as the possibility that HED patients have foreign body granulomas in the bullae. Lysozyme is detectable in human nasal lavage [35] and middle ear fluids [36] and reduced levels of lysozyme P may be a useful biomarker for auditory tube gland failure in HED patients.

HED mouse models have potential for pre-clinical testing of therapies for nasal and middle ear disease. EDAR signalling agonists improve tracheal gland function and bronchus mucociliary clearance in the X-linked HED dog [24,37] and

saliva production in radiation-injured salivary glands of FVB mice [38]. Furthermore, HED phenotypes are rescued in *Eda*^{Ta} mice born to mothers treated during pregnancy [39]. In future studies it will be important to tease apart the effect of developmental loss of glands from potential roles of EDAR signalling in the function of adult nasal glands. The expression of *Edar* in adult glands suggests the possibility that gland function may be enhanced by treatment with EDAR signalling agonists. Based on our findings in HED mice, EDAR signalling agonists, as well as symptomatic treatments such as nasal humidification and antibiotics [9] and reduction of airborne particulate load, have potential therapeutic value for treating middle ear and nasal pathology in ectodermal dysplasias.

Materials and Methods

Mice

These studies were performed under the authority of the appropriate UK Home Office Project Licence. *Downless* mice (Edar p.E379K) were maintained by intercrossing *Edar*$^{dlJ/+}$ mice; *Edar*$^{dlJ/dlJ}$ mice have a sparse hair coat, hairless tail and terminal tail kink whereas *Edar*$^{dlJ/+}$ littermates have a wild-type appearance. *Tabby* mice (*Eda*$^{Ta/Ta}$ females and *Eda*$^{Ta/Y}$ hemizygous males; collectively termed *Eda*^{Ta}) were maintained as a homozygous line. *Edar*$^{Tg951/951}$ mice were maintained as a homozygous line. FVB are the background inbred genetic line for both *Eda* and *Edar* mutant strains. Heterozygous *Mecom*$^{Jbo/+}$ mice hereafter referred to as *Junbo* mice are congenic on a C3H/HeH genetic background (European Mouse Mutant Archive; EM:00091) and maintained by crossing *Junbo* heterozygote males with C3H/HeH females [14]. *Junbo* mice bear a mutation in the transcription factor *Mecom* that disrupts its role as an inducible negative regulator of NF-kB causing an increase in responsiveness to

inflammatory stimuli [40] and develop otitis media spontaneously in specific pathogen free (SPF) conditions [14].

Specific pathogen free colony mice were housed in individually ventilated cages (IVC's) (Tecniplast) under a 12-h light/12-h dark cycle, in a temperature range of 21 ± 2^{o}C and humidity of 55 ± 10% with 15-20 changes of HEPA filtered air per hour. Mice are fed irradiated Teklad 18% Protein Rodent Diet (Harlan UK Ltd) and provided with 0.2 µm-filtered water. Mice are housed on autoclaved Aspen Chip Grade 6 bedding and cage enrichment products include Aspen wood blocks, cardboard and plastic nesting materials.

The Roslin Institute small animal facility SPF barrier was established in 2011 by embryo rederivation into specific pathogen free B6CBAF1/J hybrid recipient females. Specific pathogen free FVB mice are obtained from a commercial supplier and brought directly into the barrier, while the specific pathogen free *Junbo* colony was imported without rederivation from a separate SPF facility after extensive testing in quarantine facility. Microbiological surveillance of sentinel mice followed Federation of European Laboratory Animal Science Associations (FELASA) screening guidelines and the Roslin Institute facility is free from FELASA listed murine mouse viruses and bacterial pathogens.

Histology, immunohistochemistry, in situ hybridization and cytology

Mouse middle ear development is complete by post-natal day 15 (P15) [41]. We examined the nasal passages and bullae of 3-week-old (P20-P23) weaning-aged mice and adult mice aged 7-47 weeks of age. In vivo labelling for hypoxia was performed in *Eda*^{Ta} (n=5, 12 or 19 weeks-old) and FVB mice (n=4, 8-weeks-old) by i.p. injection of pimonidazole (Hypoxyprobe™ NPI Inc). Mice were euthanized using a rising concentration of CO_2 then decapitated.

The head was skinned and the tympanic membrane was viewed under 10X binocular magnification to diagnose gross otitis media by tympanic membrane opacity. The heads were immersion fixed in neutral buffered formalin for 48 h then decalcified in EDTA for 5-7 days; the exception was for in situ hybridization, when fixation was for 24 h and the skull base sawn into a small block to decalcify in 48 h.

Four µm wax sections of the rostral, mid and caudal nose [13], coronal and dorsal plane sections of the nasopharynx, auditory tubes and bulla, and mid sagittal sections of the larynx were cut and stained with H&E, Giemsa or Alcian Blue/PAS. The terminology used to describe the nasal submucosal glands is that by May and Tucker [42]. Histology was scored for the presence (or absence) of mucosal inflammation/thickening and intraluminal inflammatory exudate. Blinding for genotype is not possible because HED mutants have distinctive gland anatomy. Hyaline droplet degeneration [13] was assessed by counting affected epithelial cells in nasal septum in rostral and mid nose sections and proximal nasopharynx duct.

For quantitative measurement of the auditory tube lumen profiles, the skull base blocks were wax embedded ventral surface down before trimming on the microtome to produce a symmetrical dorsal plane profile on the wax block face. Specimens were then re-embedded in groups of two or three and sectioned in 50 µm dorsal plane steps starting from nasopharynx tube, up through to the entrance of the auditory tubes into the bulla. For each step section the auditory tube lumen was measured from H&E slide scan (see below) to generate a cumulative area of multiple levels.

Immunohistochemistry was performed for lysozyme, the macrophage marker F4/80, cleaved caspase 3 and the hypoxia tracer pimonidazole (Table S3). In situ hybridization for *Edar* mRNA was performed following the manufacturer's

instructions (Mm-Edar, Advanced Cell Diagnostic, catalogue number 423011) using the HRP visualization kit and performed alongside along a positive control for RNA integrity (*PpiB*) and a negative hybridization control (*DapB*) (Advanced Cell Diagnostic).

Giemsa stained cytospin cytology preparations were made from aliquots of PBS washes of nasal passages and bullae (see below) and preserved with Cytospin collection fluid (Thermo Scientific). Leukocytes were counted in ten randomly chosen 40X objective fields and their total number calculated from the proportions of cytospin area assessed and sample volume used. Leukocyte differentials were performed on 200 cells. Alternatively fresh PBS cytospin preparations were formalin fixed and stained with Oil Red O (ORO) for neutral lipid. All histology and cytology was performed in Easter Bush Pathology laboratories that are UK NEQAS accredited.

Bright field images were acquired using a Hamamatsu NanoZoomer slide scanner, or on an Olympus BX41 microscope equipped with a DP72 camera and Cell D software. NanoZoomer software was used to measure bulla foreign body particle size and auditory tube lumen profiles.

Microbiology of the nose and bullae

The nasal passages/nasopharynx of 12-13 week-old litter/cage mate $Edar^{dlJ/dlJ}$ (n=9) and $Edar^{dlJ/+}$ (n=6) mice; Eda^{Ta} mice (n=10, 12-14 weeks-old); FVB mice (n=12, 12 or 23 weeks-old); and *Junbo* mice (n=7, 18-22 weeks-old) were sampled post mortem by washing with two 100 µl aliquots of sterile PBS [17]. Healthy air-filled bullae and fluid-containing bullae were washed three times with 2 µl sterile PBS via a perforation made in the tympanic membrane and the aliquots added back to 200 µl of PBS. Twenty µl aliquots or 1:10 dilutions of the PBS samples were spread on blood

agar plates, 3% blood agar plates (to suppress *Proteus mirabilis* swarming) and MacConkey plates for colony counts.

FACS and phagolysosome formation analysis

FACS was performed on leukocytes isolated from spleen, bone marrow, peritoneum and peripheral blood from littermate $Edar^{dlJ/dlJ}$ and $Edar^{dlJ/+}$ mice on an LSR-Fortessa flow cytometer (BD Biosciences). Peritoneal macrophages from Eda^{Ta} mice and littermate $Edar^{dlJ/dlJ}$ and $Edar^{dlJ/+}$ mice, and bulla fluid neutrophils and macrophages from $Edar^{dlJ/dlJ}$ and Eda^{Ta} mice, were treated with pHrodoRed *E. coli* Bioparticle conjugate according to the manufacturer's instructions to assess phagocytosis and acidification of the phagolysosome (Table S3). In addition, bulla macrophages were imaged by fluorescent microscopy. Eda^{Ta} bulla fluid samples (n=11) were pooled in 400 µl of PBS. 200 µl aliquots were plated in wells of a 12 well flat bottom, polystyrene tissue culture plate containing 1.5ml complete RPMI medium (RPMI media containing 10% FCS and Penicillin Streptomycin). pHrodoRed *E. coli* was added to one well and the plate incubated for 2 h in 5% CO_2 at 37°C. An untreated well served as negative control for cell autofluorescence. The plate was imaged with an Eclipse TE2000 Inverted Microscope (Nikon) to obtain phase contrast and fluorescent images.

Statistical analysis

The statistical tests were chosen after D'Agostino & Pearson omnibus normality tests, and are given in results and/or figure legends. Data are presented in graphs as individual data points and median or mean. Disease prevalence data was analyzed using Chi-squared or Fisher's exact tests and graphically represented as histogram bars. Two-tailed tests were used throughout and test values $P<0.05$ were considered

to be statistically significant. Graphs and statistics were generated using Prism Graph Pad or SAS.

Funding

This work was supported by a BBSRC Institute Strategic Programme Grant to the Roslin Institute.

Acknowledgements

We thank Alex Robertson and Kris Hogan for the husbandry of the mice; Neil Macinctyre, Sharon Moss, Dawn Drummond, Gillian McGregor and Nikki Fraser for performing the histology, immunohistochemistry and cytology; and Jennifer Harris and Claire Taylor for performing the bacteriology.

Reference list

1. Sadier,A., Viriot,L., Pantalacci,S., and Laudet,V. (2014)The ectodysplasin pathway: from diseases to adaptations. *Trends Genet.* 30, 24-31.

2. Majumder,K., Shawlot,W., Schuster,G., Harrison,W., Elder,F.F. and Overbeek,P.A. (1998) YAC rescue of downless locus mutations in mice. *Mamm. Genome.*, **9**, 863-868.

3. Mou,C., Thomason,H.A., Willan,P.M., Clowes,C., Harris,W.E., Drew,C.F., Dixon,J., Dixon,M.J. and Headon,D.J. (2008) Enhanced ectodysplasin-A receptor (EDAR) signaling alters multiple fiber characteristics to produce the East Asian hair form. *Hum. Mutat.,* **29**, 1405-1411

4. Chang,S.H., Jobling, S., Brennan, K. and Headon, D.J. (2009) Enhanced Edar signalling has pleiotropic effects on craniofacial and cutaneous glands. *PLoS, One,* **4**, e7591.

5. Mehta,U., Brunworth,J., Lewis,R.A. and Sindwani,R. (2007) Rhinologic manifestations of ectodermal dysplasia. *Am. J. Rhinol.,* **21**, 55-58.

6. Henningsen,E., Svendsen,M.T., Lildballe,D.L. and Jensen,P.K. (2014) A novel mutation in the EDAR gene causes severe autosomal recessive hypohidrotic ectodermal dysplasia. *Am. J. Med. Genet. A*., **164A**, 2059-2061.

7. Martini,A., Magnan,G. and Peserico,A. (1984) Ozena as presenting symptom of a rare and severe genetic disease: hypohidrotic ectodermal dysplasia. *Int. J. Pediatr. Otorhinolaryngol.,* **8**, 97-103.

8. Mehta,U., Brunworth,J., Fete,T.J. and Sindwani,R. (2007) Head and neck manifestations and quality of life of patients with ectodermal dysplasia. *Otolaryngol. Head Neck Surg.,* **136**, 843-847.

9. Callea,M., Teggi,R., Yavuz,I., Tadini,G., Priolo,M., Crovella S., Clarich,G. and Grasso,D.L. (2013) Ear nose throat manifestations in hypoidrotic ectodermal dysplasia. *Int, J, Pediatr, Otorhinolaryngol*., **77**, 1801-1804.

10. Shin,J.J. and Hartnick,C.J. (2004) Otologic manifestations of ectodermal dysplasia. *Arch, Otolaryngol, Head Neck Surg.,* **130**, 1104-1107.

11. Grüneberg,H. (1971) The glandular aspects of the tabby syndrome in the mouse. *J. Embryol. Exp. Morphol.,* **25**, 1-19.

12. Trokovic,N., Pöllänen,R., Porola,P., Stegaev,V., Hetzel,U., Tivesten,Å., Engdahl, C., Carlsten,H., Forsblad-d'Elia,H., Fagman,J.B., et al. (2012) Exosomal secretion of death bullets: a new way of apoptotic escape? *Am. J. Physiol. Endocrinol. Metab*., **303**, E1015-1024.

13. Herbert, R.A., Leninger, J.R. (1999) Nose, larynx and trachea. In Maronpot, R.R., Boorman, G.A., Gaul, B.W. (eds), *Pathology of the Mouse: Reference and Atlas*. Cache River Press, Vienna, USA, pp. 259-292.

14. Parkinson,N., Hardisty-Hughes,R.E., Tateossian,H., Tsai,H.T., Brooker,D., Morse,S., Lalane,Z., MacKenzie,F., Fray,M., Glenister,P. et al. (2006) Mutation at the Evi1 locus in Junbo mice causes susceptibility to otitis media. *PLoS, Genet.,* **2**, e149.

15. Cheeseman,M.T., Tyrer,H.E., Williams,D., Hough,T.A., Pathak,P., Romero,M.R., Hilton,H., Bali,S., Parker,A., Vizor,L., et al. (2011) HIF-VEGF pathways are critical for chronic otitis media in Junbo and Jeff mouse mutants. *PLoS. Genet.,* **7**, e1002336.

16. Bhutta,M.F., Cheeseman,M.T. and Brown,S.D. (2014) Myringotomy in the Junbo mouse model of chronic otitis media alleviates inflammation and cellular hypoxia. *Laryngoscope*. **124**, E377-383.

17. Hood,D., Moxon,R., Purnell,T., Richter,C., Williams,D., Azar,A., Crompton,M., Wells,S., Fray,M., Brown,S.D. et al. (2016) A new model for non-typeable Haemophilus influenzae middle ear infection in the Junbo mutant mouse. *Dis. Model. Mech.,* **9**, 69-79.

18 . Rawlins,E.L., Hogan,B.L. (2005) Intercellular growth factor signaling and the development of mouse tracheal submucosal glands. *Dev. Dyn.,* **233**, 1378-1385.

19. Kalogjera,L., Pegan,B., Petric,V. (1991) Compensatory mechanisms induced by high oropharyngeal airway resistance in rats. *Acta. Otolaryngol.,* **111**, 384-388.

20. Park,K., Lim,D.J. (1993) Development of secretory elements in murine tubotympanum: lysozyme and lactoferrin immunohistochemistry. *Ann. Otol. Rhinol. Laryngol.,* **102**, 385-395.

21. Lim,D.J., Chun,Y.M., Lee,H.Y., Moon,S.K., Chang,K.H., Li, J.D. and Andalibi,A. (2000) Cell biology of tubotympanum in relation to pathogenesis of otitis media - a review. *Vaccine,* **19** Suppl 1, S17-25.

22. Markart,P., Faust,N., Graf,T., Na,C.L., Weaver,T.E. and Akinbi,H.T. (2004) Comparison of the microbicidal and muramidase activities of mouse lysozyme M and P. *Biochem. J.*, **380**, 385-392.

23. Shimada,J., Moon,S.K., Lee,H.Y., Takeshita,T., Pan,H., Woo,J.I., Gellibolian,R., Yamanaka,N. and Lim,D.J. (2008) Lysozyme M deficiency leads to an increased susceptibility to Streptococcus pneumoniae-induced otitis media. *BMC. Infect. Dis.,* **8**, 134.

24. Casal,M.L., Lewis,J.R., Mauldin,E.A., Tardivel,A., Ingold,K., Favre,M., Paradies,F., Demotz,S., Gaide,O. and Schneider,P. (2007) Significant correction of disease after postnatal administration of recombinant ectodysplasin A in canine X-linked ectodermal dysplasia. *Am. J. Hum. Genet.,* **81**, 1050-1056.

25. Corcoran,T.E. (1985) A better picture of clearance in the nose. *J. Appl. Physiol. (1985).*, **108**, 1-2.

26. Hisamatsu,K., Yamauchi,Y., Uchida,M. and Murakami,Y. (1986) Promotive effect of lysozyme on the ciliary activity of the human nasal mucosa. *Acta, Otolaryngol.,* **101**, 290-294.

27. St. Clare,M.B.G. and Morgan, K.T. (1992) Changes in the Upper Respiratory Tract. In Mohr,U., Dungworth, CC and Capen,CC (eds.), *Pathobiology of the Aging Rat.* ILSI Press Washington, DC, USA, Vol. 1, pp. 111-127.

28. Melo,R.C., Dvorak,A.M. (2012) Lipid body-phagosome interaction in macrophages during infectious diseases: host defense or pathogen survival strategy? *PLoS. Pathog.,* **8**, e1002729.

29. Wiese,M., Gerlach,R.G., Popp,I., Matuszak,J., Mahapatro,M., Castiglione,K., Chakravortty,D., Willam,C., Hensel,M., Bogdan,C., et al. (2012) Hypoxia-mediated impairment of the mitochondrial respiratory chain inhibits the bactericidal activity of macrophages. *Infect. Immun.*, **80**, 1455-1466.

30. Casal,M.L., Mauldin,E.A., Ryan,S., Scheidt,J.L., Kennedy,J., Moore,P.F. and Felsburg,P.J. (2005) Frequent respiratory tract infections in the canine model of X-linked ectodermal dysplasia are not caused by an immune deficiency. *Vet. Immunol. Immunopathol.*, **107**, 95-104.

31. Fuchs,J.C., Linden,J.F., Baldini,A. and Tucker,A.S. (2015) A defect in early myogenesis causes Otitis media in two mouse models of 22q11.2 Deletion Syndrome. *Hum. Mol. Genet.*, **24**, 1869-1882.

32. Noben-Trauth,K. and Latoche,J.R. (2011) Ectopic mineralization in the middle ear and chronic otitis media with effusion caused by RPL38 deficiency in the Tail-short (Ts) mouse. *J. Biol. Chem.,* **286**, 3079-3093.

33. Cayé-Thomasen,P. and Tos,M. (2004) Eustachian tube gland tissue changes are related to bacterial species in acute otitis media. *Int. J. Pediatr. Otorhinolaryngol.,* **68**, 101-110.

34. Parker,D. and Prince,A. (2011) Innate immunity in the respiratory epithelium. *Am. J. Respir. Cell Mol. Biol*., **45**, 189-201.

35. Ghafouri,B., Ståhlbom,B., Tagesson,C.and Lindahl,M. (2002) Newly identified proteins in human nasal lavage fluid from non-smokers and smokers using two-dimensional gel electrophoresis and peptide mass fingerprinting. *Proteomics*, **2**, 112-120

36. Juhn,S.K., Giebink,G.S., Huff,J.S. and Mills, E.L. (1980) Biochemical and immunochemical characteristics of middle ear effusions in relation to bacteriological findings. *Ann. Otol. Rhinol. Laryngol. Suppl*., **89**,161-167.

37. Mauldin,E.A., Gaide,O., Schneider,P. and Casal,M.L. (2009) Neonatal treatment with recombinant ectodysplasin prevents respiratory disease in dogs with X-linked ectodermal dysplasia. *Am. J. Med. Genet. A,* **149A**, 2045-2049.

38. Hill,G., Headon,D., Harris,Z., Huttner,K. and Limesand, K.H. (2014) Pharmacological activation of the EDA/EDAR signaling pathway restores salivary gland function following radiation-induced damage. *PLoS. One,* **9**, e112840.

39. Kowalczyk,C., Dunkel,N., Willen,L., Casa,M.L., Mauldin,E.A., Gaide,O., Tardivel,A., Badic,G., Etter,A.L., Favre,M., et al. (2011) Molecular and therapeutic characterization of anti-ectodysplasin A receptor (EDAR) agonist monoclonal antibodies. *J. Biol. Chem.* **286**, 30769-30779.

40. Xu,X., Woo,C.H., Steere,R.R., Lee,B.C., Huang,Y., Wu,J., Pang,J., Lim,J.H., Xu,H., Zhang,W., et al. (2012) EVI1 acts as an inducible negative-feedback regulator of NF-κB by inhibiting p65 acetylation. *J. Immunol.,* **188**, 6371-6380.

41. Park,K., Ueno,K. and Lim,D.J. (1992) Developmental anatomy of the eustachian tube and middle ear in mice. *Am. J. Otolaryngol.,* **13**, 93-100.

42. May,A. and Tucker,A. (2015) Understanding the development of the respiratory glands. *Dev. Dyn*., **244**, 525-539.

Figure Legends

Figure 1. Anatomy and histology of the nasopharynx in EDA pathway deleted mice. (A-D) Dorsal plane sections, E-L coronal sections. (A) FVB wild-type controls, *Edar*$^{dlJ/+}$ and *Edar* $^{Tg951/951}$ mice have submucosal glands (smg) located in caudal region of the nasopharynx duct (nd) associated with the auditory tubes (at) that connect the nasopharynx duct to the bulla (b); (B) is at higher magnification of this region. (C) Small nasopharynx submucosal glands (smg) are located caudal to the opening of the auditory tubes, the example shown is a 16-week-old *Edar*$^{dlJ/+}$ mouse; (D) caudal nasopharynx glands are absent *Edar*$^{dlJ/dlJ}$ and *Eda*^{Ta} mice; the example shown is a 12-week-old *Eda*^{Ta} mouse. (E) Coronal section of the nasopharynx in a 37-week-old FVB mouse shows auditory tube submucosal glands (smg) and submucosal glands in the soft palate (arrow); (G, I) auditory tube submucosal glands shown at higher magnifications have serous cells and mucous cell populations, and the auditory tubes have Alcian Blue positive goblet cells (arrowheads); stained with PAS Alcian Blue. (F, H, J) Comparable sections in a 27-week-old *Eda*^{Ta} mouse lacking submucosal glands and auditory tube goblet cells: note foreign body (fb) in the nasopharynx duct. (K) In the FVB mouse the submucosal gland serous gland cell population (arrows), and the auditory tube epithelium secretory cells (arrowheads) stain positively for lysozyme. (L) In the *Eda*^{Ta} mouse, lysozyme positive myeloid cells (mc) in the bone marrow cavity and auditory tube lumen. Scale bars: 2.5 mm (A); 1.0 mm (B); 500 µm (C, D, E, F); 250 µm (G, H, K, L); 100 µm (I, J).

Figure 2. Nasal glands in EDA pathway deleted mice and *Edar* expression in adult glands. (A-L) are coronal sections. (A) Submucosal glands in the mid region of the nose of a 37-week-old FVB mouse, medial nasal glands (mng) are located in the mucosa either side of the nasal septum; and lateral nasal glands (lng) are located in

the lateral walls of the nasal chambers; PAS Alcian Blue. (B) Higher magnification of the lateral nasal gland; (C) higher magnification of the medial nasal gland and both nasal glands are comprised solely of serous cells; note that PAS-positive amorphous amyloid material (arrow) between submucosal gland acini is an incidental degenerative change in the medial nasal glands of older mice: see reference [13]. (D) Higher magnification of the lateral nasal glands shows a ventral area stains weakly with PAS. (E) Medial nasal gland and (F) lateral nasal gland in the FVB mouse do not stain for lysozyme; note that the nasal septum cartilage chondrocytes are lysozyme positive. Medial nasal glands in the rostral (G) and (H) mid nose regions in FVB and *Edar*$^{dlJ/dlJ}$ mice stain positively for cleaved caspase 3 (arrows), example shown in 3-week-old FVB mouse. (I-K) In situ hybridization detecting *Edar* mRNA in 3-week-old *Edar* $^{Tg951/951}$. (I) Nasopharynx and (J) soft palate gives punctate signals (arrows) in the nasopharynx and soft palate submucosal glands and duct, nasopharynx and auditory tube ciliated epithelium, and squamous epithelium of the oral cavity. There are no hybridization signals in muscle (m). (K) Higher magnification of the *Edar* signals in auditory tube submucosal gland and epithelium (e). (L) There are no hybridization signals using the negative control probe *DapB*. Scale bars: 2.5 mm (A); 500 µm (B); 500 µm (C, D, E, F); 100 µm (I, J); 20 µm (K, L).

Figure 3. Pathology of the nose and nasopharynx in EDA pathway deleted mice. (A) Rhinitis, nasopharyngitis and otitis media increases in prevalence between weaning age (3 weeks) and adulthood in *Edar*$^{dlJ/dlJ}$ (7-17 weeks old) and *Eda*^{Ta} (12-43 week old) mice: there was no evidence of this pathology in *Edar*$^{dlJ/+}$ (n=45), *Edar* $^{Tg951/951}$ (n=23) or FVB (n=36) mice. The number above each histogram bar indicates the number of tissues examined. (B) The number of nasal epithelial cells with hyaline

droplets in rostral, mid and nasopharynx duct sections is higher in *Edar*$^{dlJ/dlJ}$ and *Eda*^{Ta} mice compared to FVB and *Edar*$^{dlJ/+}$ respectively at 3-weeks (weaning) and 12-weeks of age. The graph represents data points and the median (that incudes zero values) as a bar; two-tailed Kruskal Wallis test; **P*<0.05, ***P*<0.01, *****P*< 0.001 Dunn's multiple comparison test. (C) The rostral nasal passages of a 21-day-old *Eda*^{Ta} mouse with rhinitis contain foreign bodies (fb hair shaft fragments and plant material) mixed with neutrophil rich exudate (ex); medial submucosal gland (mng) and nasal septum cartilage (nsc). (D) Comparable image of 22-day-old FVB mouse shows no evidence of intraluminal exudate. (E) Ciliated epithelial cells with intracytoplasmic hyaline droplets (hd) and cytoplasmic blebbing (cb) in the nasal septum of a 12-week-old *Eda*^{Ta} mouse; Giemsa stain. (F) Comparable section in a 12-week-old FVB mouse shows normal respiratory epithelium without hyaline droplets. (G) Nasopharyngitis in 21-day-old *Edar*$^{dlJ/dlJ}$ mouse with squamous epithelium (se) lining the roof of the nasopharynx (nd) and infiltration of the submucosa with lymphocytes and plasma cells (pc); (I) shows higher magnification of the squamous epithelium (H) The nasopharynx of 21-day-old FVB mouse has a ciliated respiratory epithelium (ce) with goblet cells, and auditory tube submucosal glands (smg); (J) shows a higher magnification of the ciliated epithelium. Scale bars 100 µm (C, D, G, H); 50 µm (E, F); 20 µm (I, J).

Figure 4. Pathology of the auditory bulla in EDA pathway deleted mice. (A) The healthy air filled bulla (b) and auditory tube (at) in a 37-week-old FVB mouse; note auditory tube submucosal glands (smg). (B) Higher magnification image (A) shows the bulla mucosa in the region adjacent to the auditory tube opening has ciliated epithelium (ce). (C) A 43-week-old *Eda*^{Ta} mouse with otitis media has exudate (ex) in

the bulla lumen and auditory tube and (D) epithelium adjacent to the auditory tube opening, has goblet cell hyperplasia (gch). (E, F) In-vivo labelling with the hypoxia tracer pimonidazole shows positive staining in epithelium (e) and bulla foamy macrophages (fm) in a representative 16-week-old *Eda*^{Ta} mouse. (F) Hypoxia signals are absent in the healthy air-filled bulla of a representative 8-week-old FVB control mouse. (G, H) The caudal bulla lumen of an 11-week-old *Edar*$^{dlJ/dlJ}$ mouse has an organized vascular granuloma (g) surrounded by exudate (ex) containing neutrophils and foamy macrophages (fm); bulla mucosa (m). (H) Higher magnification of image (G) shows the granuloma has an epithelial margin (e), embedded foreign body (fb) and capillaries (c). Macrophages in the granuloma and foamy macrophages (fm) in bulla exudate give stain positively for F4/80. (I) A granuloma located in the caudal bulla of a 14-week-old *Eda*^{Ta} mouse has PAS positive (plant-based) foreign body particle (fb) at the margin. (J) Hair shaft fragments (fb) in the neutrophil rich exudate (ex) of a 43-week-old *Eda*^{Ta} mouse; note plasma cell (pc) infiltration of the thickened bulla mucosa (m). Scale bars: 500 µm (A, C); 50 µm (B, D); 100 µm (E, F, H, J), 200 µm (G) 250 µm (I)

Figure 5. Auditory tube gating function is compromised in the absence of submucosal glands. (A) Coronal section of the rostral nose in a *Junbo* mouse has normal air filled nasal passages; note vomeronasal organ (vno). (B-D) Dorsal plane sections. (B) The opening of the auditory tube (at) into the nasopharynx (nd) in a *Junbo* mouse shows the normal mucosa of the nasopharynx is lined by ciliated epithelium (ce). (C, D) Nasopharynx (nd), auditory tubes (at) and bullae (b). (C) An auditory tube in a 45-week-old *Junbo* mouse with a slender profile and empty lumen; note submucosal glands (smg). (D) The auditory tube of a 13-week-old *Eda*^{Ta} mouse

contains exudate (ex) and hair shaft foreign body material (fb) (inset shows higher magnification of the tube contents). (E) Auditory tube lumen area is significantly greater in Eda^{Ta} (n=6 mice, 13-weeks-old) than in $Edar^{dlJ/dlJ}$ (n=6 mice, 16-weeks-old), $Edar^{dlJ/+}$ (n=6 mice, 15-16 weeks-old) and *Junbo* (n=5 mice, 24-45 weeks-old). Total area for each auditory tube was measured in 50 µm step sections, and data are represented as points with the average as a bar; one-way ANOVA and Tukey's multiple comparison test; **** $P<0.0001$. (F) Bulla foreign body particle size in $Edar^{dlJ/dlJ}$ and Eda^{Ta} mice is significantly larger than in *Junbo* mice. Particle sizes were measured in the bullae of $Edar^{dlJ/dlJ}$ (n=11 mice, 7-17 weeks old), Eda^{Ta} (n=10, 13-30 weeks old) and *Junbo* (n=9, 14-45 weeks old) mice. The graph represents data points and the median as a bar; 2-tailed Kruskal Wallis test; ****$P<0.0001$ and NS not significant in Dunn's multiple comparison test.

Scale bars: 250 µm (A, B); 500 µm (C, D); 100 µm (panel D inset).

Figure 6. Commensal bacteria populations and inflammatory response in the nose and auditory bulla of EDA pathway deleted mice. (A) Leukocyte numbers in the nasal wash of $Edar^{dlJ/dlJ}$ and Eda^{Ta} mice are significantly elevated (see text for details) compared to FVB, $Edar^{dlJ/+}$ and *Junbo* mice. (B) Total bacterial load (CFU) in nasal samples are significantly elevated (see text for details) in $Edar^{dlJ/dlJ}$ (predominately *E. coli*) and Eda^{Ta} (predominately *Staphylococcus aureus*) mice than FVB, $Edar^{dlJ/+}$ and *Junbo* mice. (C) Cocci colonies (c) associated with plant foreign body (fb) in the nasopharynx (nd) at the opening of the auditory tube (at) of a 43-week-old Eda^{Ta} mouse. (D) Total bacterial load in bulla samples was highest in $Edar^{dlJ/dlJ}$ (predominately *E. coli*) and *Junbo* (mixed bacterial isolates, see Table S1 for bacterial isolate list). (E) Giemsa stained cytology of bulla exudate from an *E. coli*

culture positive 11-week-old *Edar*$^{dlJ/dlJ}$ mouse shows a foamy macrophage with bacilli (ba); (F) a histology section shows the Gram-negative bacilli (ba) are intracytoplasmic; F4/80 IHC (Vector SG detection kit has a blue-grey chromogen) and Neutral Red counterstain. (G) Bulla foamy macrophages from a 13-week-old *Eda*^{Ta} mouse contain lipid bodies; formalin fixed cytology preparation stained with Oil Red O. (A, B, D) The graphs represent data points, the median (that incudes zero values) as a bar, and the ratio above each represents the number of positive samples divided by the total number sampled. Scale bars: 100 µm (C); 20 µm (E, F); 50 µm (G).

Figure 7. Immune cell populations and function in EDA pathway deleted mice. (A, B) Peritoneal macrophages. (A) A Forward Scatter (FSC) Side Scatter (SCS) plot shows the selected peritoneal macrophage population from an *Edar*$^{dlJ/+}$ mouse. The overlay histogram shows pHrodoRed fluorescence in the macrophage gate for a control sample incubated at 4°C to inhibit phagocytosis (blue) and sample incubated at 37°C (red). (B) FSC^{High} F4/80^{High} gated peritoneal macrophages analyzed for pHrodoRed fluorescent signals. (C-G) Bulla fluid leukocytes from *Edar*$^{dlJ/dlJ}$ mice. (C) FSC SSC selected leukocytes were analysed in a F4/80 Ly6g plot and 85.6% of the leukocytes were Ly6g^{High} F4/80^{Low} neutrophils (n) (median 95% CI 71.7-94.6%) and 2.1% were Ly6g^{High} F4/80^{High} macrophages (m) (95% CI, 1.2-3.5%). (D) FSC SSC plots were used to select two leukocyte populations. The FSC^{Low} SSC^{Low} gated leukocytes had 23.9% PI^{-} AnnexinV^{-} viable cells (v) (median 95% CI 11.1-52.3) and 74% PI^{+}AnnexinV^{+} apoptotic or necrotic cells (anc) (95% CI 41.6-76.3%). The FSC^{High} SSC^{High} gated leukocytes had 86.1% PI^{-} AnnexinV^{-} viable cells (median, 95% CI, 84.0-97.0) and 11.6% PI^{+}AnnexinV^{+} apoptotic or necrotic cells (95% CI 1.8-

11.9%). (E-G) The overlay histograms for pHrodoRed fluorescence. (E) FSC^{Low} SSC^{Low} selected leukocytes (blue) have a low population of viable cells capable of phagocytosis, whereas FSC^{High} SSC^{High} selected leukocytes (red) have high population of viable cells capable of phagocytosis. (F) A FSC^{High} SSC^{High} selected PI^{-} $AnnexinV^{-}$ viable leukocytes incubated at 37°C show a phagocytosis signal (red) but incubation at 4°C (blue) inhibits phagocytosis. (G) 56% of $Ly6g^{High}F4/80^{Low}$ neutrophils (95% CI 50-71%) (red) were phagocytically active and 72% of $Ly6g^{High}F4/80^{High}$ macrophages (95% CI, 59-93%) (blue) were phagocytically active. (H, I) Eda^{Ta} mouse bulla leukocytes; (H) phase contrast image of cells; (I) pHrodoRed fluorescent image of the same field of view, the smaller cells are the same size as neutrophils (n), and larger cells are macrophages and foamy macrophages (fm). The untreated control had no detectable autofluorescent signal. Scale bar 50 μm. (J) The percentage of pHrodoRed positive peritoneal macrophages was not significantly different in Eda^{Ta}, $Edar^{dlJ/dlJ}$, $Edar^{dlJ/+}$ mice (Kruskal Wallis test); whereas the percentage of positive bulla neutrophils and macrophages was significantly higher in Eda^{Ta} than $Edar^{dlJ/dlJ}$ mice. The graph represents data points and the median as a bar. NS $P>0.05$; ** $P<0.01$.

Figure 8. Larynx histology and aerophagia in EDA pathway deleted mice

A-D larynx mid-sagittal plane. (A) The epiglottis (e) of a 24-week-old FVB mouse has submucosal glands (smg) but these are absent in $Edar^{dlJ/dlJ}$ and Eda^{Ta} mice; (B) the epiglottis of 14-week-old $Edar^{dlJ/dlJ}$ mouse lacks glands and has a submucosal lymphoid follicle (lf); there is exudate (ex) and foreign body (fb) in the proximal trachea. (C, D) Two 25-week-old mice Eda^{Ta} mice; (C) one Eda^{Ta} mouse has neutrophil (nl) infiltration of the epiglottis epithelium, and (D) a higher magnification

image of a submucosal lymphoid follicle (lf) in a second *Eda*^{Ta} mouse. (E, F) soft palate mid-sagittal plane. (E) The soft palate of a 24-week-old FVB mouse has submucosal gland comprising mucous cells (smg) that empty via ducts (arrow head) into the oral cavity (oc); nasopharynx (nd) is lined by ciliated epithelium (ce). (F) The soft palate of a 14-week-old *Edar*$^{dlJ/dlJ}$ mouse lacks submucosal glands and this region is occupied by adipose tissue (adp); the nasopharynx is lined by squamous epithelium (se). (G, H) trachea mid-sagittal plane. (G) The proximal trachea of a 14-week-old *Edar*$^{dlJ/+}$ mouse has submucosal glands (smg); (H) these glands are absent in a 25-week-old *Eda*^{Ta} mouse. (I) Post mortem appearance of an 18-week-old *Eda*^{Ta} mouse with aerophagia that has an air filled stomach, small intestines and caecum. (J, K) small intestine. (J) Duodenum of this *Eda*^{Ta} mouse has a normal submucosal Brunner's gland (brg) and villi (v); (K) the jejunum has an empty lumen. Scale bars: 250 μm (A, B, E-H, J, K); 100 μm (C, D).

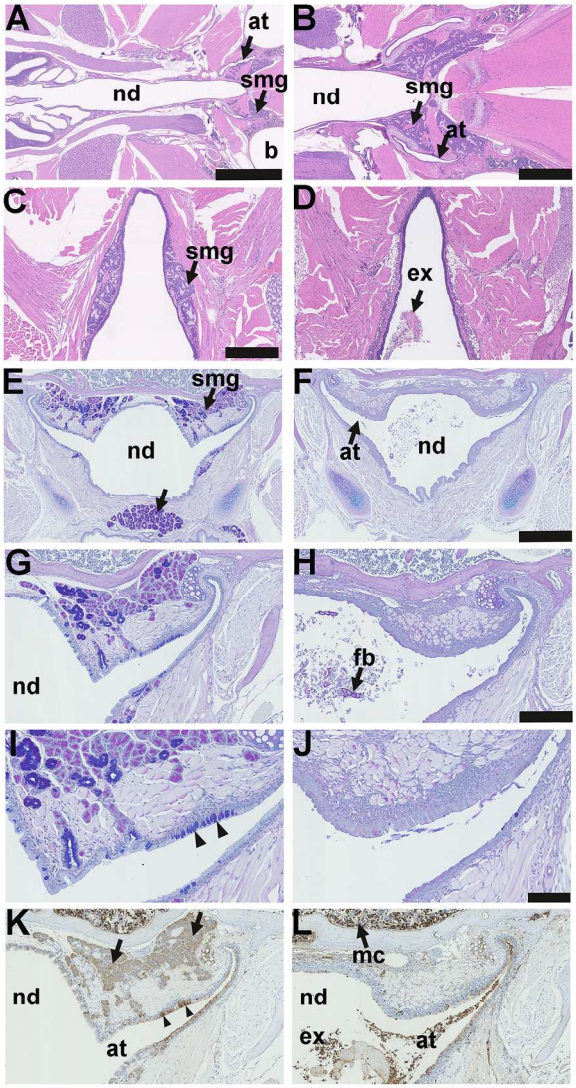

Figure 1. Anatomy and histology of the nasopharynx in EDA pathway deleted mice. (A-D) Dorsal plane sections, E-L coronal sections. (A) FVB wild-type controls, *Edar*$^{dlJ/+}$ and *Edar* $^{Tg951/951}$ mice have submucosal glands (smg) located in caudal region of the nasopharynx duct (nd) associated with the auditory tubes (at) that connect the nasopharynx duct to the bulla (b); (B) is at higher magnification of this region. (C) Small nasopharynx submucosal glands (smg) are located caudal to the opening of the auditory tubes, the example shown is a 16-week-old *Edar*$^{dlJ/+}$ mouse; (D) caudal nasopharynx glands are absent *Edar*$^{dlJ/dlJ}$ and *Eda*^{Ta} mice; the example shown is a 12-week-old *Eda*^{Ta} mouse. (E) Coronal section of the nasopharynx in a 37-week-old FVB mouse shows auditory tube submucosal glands (smg) and submucosal glands in the soft palate (arrow); (G, I) auditory tube submucosal glands shown at higher magnifications have serous cells and mucous cell populations, and the auditory tubes have Alcian Blue positive goblet cells (arrowheads); stained with PAS Alcian Blue. (F, H, J) Comparable sections in a 27-week-old *Eda*^{Ta} mouse lacking submucosal glands and auditory tube goblet cells: note foreign body (fb) in the nasopharynx duct. (K) In the FVB mouse the submucosal gland serous gland cell population (arrows), and the auditory tube epithelium secretory cells (arrowheads) stain positively for lysozyme. (L) In the *Eda*^{Ta} mouse, lysozyme positive myeloid cells (mc) in the bone marrow cavity and auditory tube lumen. Scale bars: 2.5 mm (A); 1.0 mm (B); 500 μm (C, D, E, F); 250 μm (G, H, K, L); 100 μm (I, J).
180x199mm (300 x 300 DPI)

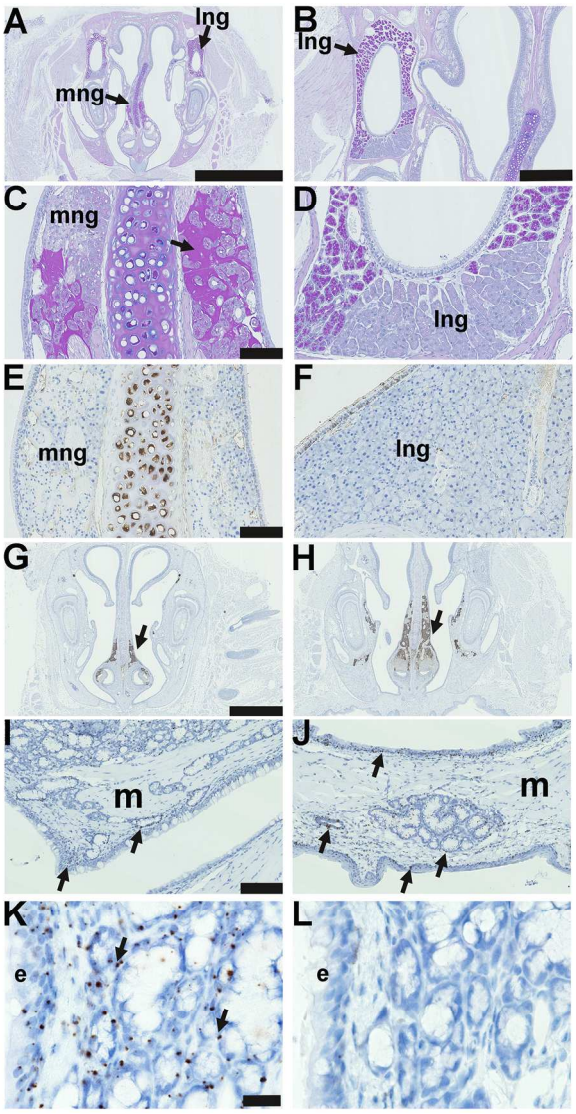

Figure 2. Nasal glands in EDA pathway deleted mice and Edar expression in adult glands. (A-L) are coronal sections. (A) Submucosal glands in the mid region of the nose of a 37-week-old FVB mouse, medial nasal glands (mng) are located in the mucosa either side of the nasal septum; and lateral nasal glands (lng) are located in the lateral walls of the nasal chambers; PAS Alcian Blue. (B) Higher magnification of the lateral nasal gland; (C) higher magnification of the medial nasal gland and both nasal glands are comprised solely of serous cells; note that PAS-positive amorphous amyloid material (arrow) between submucosal gland acini is an incidental degenerative change in the medial nasal glands of older mice: see reference [13]. (D) Higher magnification of the lateral nasal glands shows a ventral area stains weakly with PAS. (E) Medial nasal gland and (F) lateral nasal gland in the FVB mouse do not stain for lysozyme; note that the nasal septum cartilage chondrocytes are lysozyme positive. Medial nasal glands in the rostral (G) and (H) mid nose regions in FVB and *Edar*$^{dlJ/dlJ}$ mice stain positively for cleaved caspase 3 (arrows), example shown in 3-week-old FVB mouse. (I-K) In situ hybridization detecting *Edar* mRNA in 3-week-old *Edar* $^{Tg951/951}$. (I) Nasopharynx and (J) soft palate gives punctate signals (arrows) in the nasopharynx and soft palate submucosal glands and duct, nasopharynx and auditory tube ciliated epithelium, and squamous epithelium of the oral cavity. There are no hybridization signals in muscle (m). (K) Higher magnification of the *Edar* signals in auditory tube submucosal gland and epithelium (e). (L) There are no hybridization signals using the negative control probe *DapB*. Scale bars: 2.5 mm (A); 500 μm (B); 500 μm (C, D, E, F); 100 μm (I, J); 20 μm (K, L).

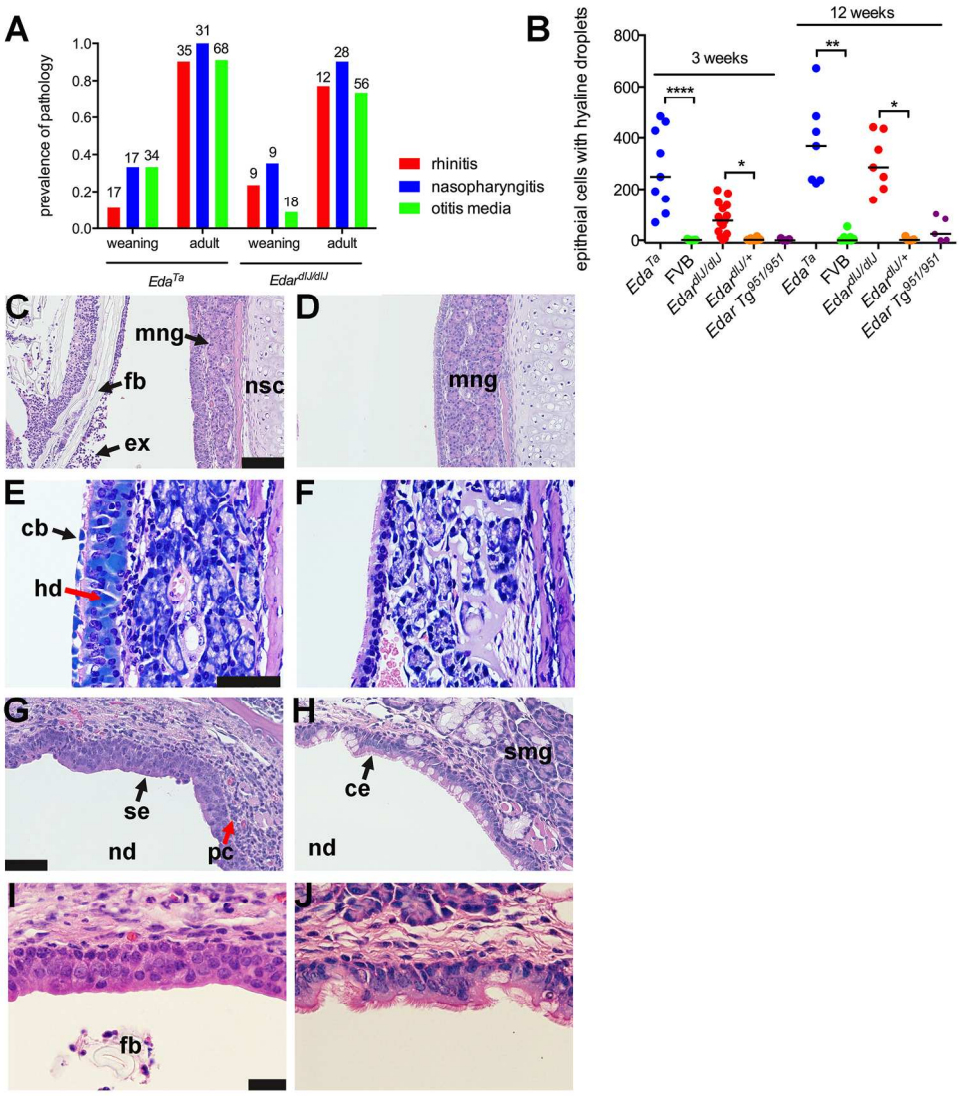

Figure 3. Pathology of the nose and nasopharynx in EDA pathway deleted mice. (A) Rhinitis, nasopharyngitis and otitis media increases in prevalence between weaning age (3 weeks) and adulthood in *Edar*$^{dlJ/dlJ}$ (7-17 weeks old) and *Eda*^{Ta} (12-43 week old) mice: there was no evidence of this pathology in *Edar*$^{dlJ/+}$ (n=45), *Edar* $^{Tg951/951}$ (n=23) or FVB (n=36) mice. The number above each histogram bar indicates the number of tissues examined. (B) The number of nasal epithelial cells with hyaline droplets in rostral, mid and nasopharynx duct sections is higher in *Edar*$^{dlJ/dlJ}$ and *Eda*^{Ta} mice compared to FVB and *Edar*$^{dlJ/+}$ respectively at 3-weeks (weaning) and 12-weeks of age. The graph represents data points and the median (that incudes zero values) as a bar; two-tailed Kruskal Wallis test; *P<0.05, **P<0.01, ****P< 0.001 Dunn's multiple comparison test. (C) The rostral nasal passages of a 21-day-old *Eda*^{Ta} mouse with rhinitis contain foreign bodies (fb hair shaft fragments and plant material) mixed with neutrophil rich exudate (ex); medial submucosal gland (mng) and nasal septum cartilage (nsc). (D) Comparable image of 22-day-old FVB mouse shows no evidence of intraluminal exudate. (E) Ciliated epithelial cells with intracytoplasmic hyaline droplets (hd) and cytoplasmic blebbing (cb) in the nasal septum of a 12-week-old *Eda*^{Ta} mouse; Giemsa stain. (F) Comparable section in a 12-week-old FVB mouse shows normal respiratory epithelium without hyaline droplets. (G) Nasopharyngitis in 21-day-old *Edar*$^{dlJ/dlJ}$ mouse with squamous epithelium (se) lining the roof of the nasopharynx (nd) and infiltration of the submucosa with lymphocytes and plasma cells (pc); (I) shows higher magnification of the squamous epithelium (H) The nasopharynx of 21-day-old FVB mouse has a

ciliated respiratory epithelium (ce) with goblet cells, and auditory tube submucosal glands (smg); (J) shows a higher magnification of the ciliated epithelium. Scale bars 100 μm (C, D, G, H); 50 μm (E, F); 20 μm (I, J).
180x199mm (300 x 300 DPI)

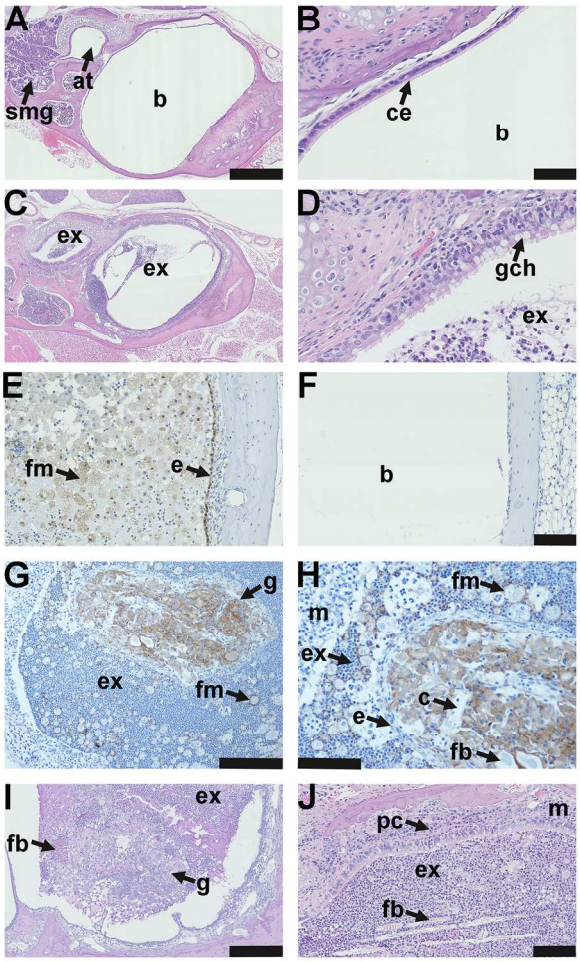

Figure 4. Pathology of the auditory bulla in EDA pathway deleted mice. (A) The healthy air filled bulla (b) and auditory tube (at) in a 37-week-old FVB mouse; note auditory tube submucosal glands (smg). (B) Higher magnification image (A) shows the bulla mucosa in the region adjacent to the auditory tube opening has ciliated epithelium (ce). (C) A 43-week-old *Eda*^{Ta} mouse with otitis media has exudate (ex) in the bulla lumen and auditory tube and (D) epithelium adjacent to the auditory tube opening, has goblet cell hyperplasia (gch). (E, F) In-vivo labelling with the hypoxia tracer pimonidazole shows positive staining in epithelium (e) and bulla foamy macrophages (fm) in a representative 16-week-old *Eda*^{Ta} mouse. (F) Hypoxia signals are absent in the healthy air-filled bulla of a representative 8-week-old FVB control mouse. (G, H) The caudal bulla lumen of an 11-week-old *Edar*$^{dlJ/dlJ}$ mouse has an organized vascular granuloma (g) surrounded by exudate (ex) containing neutrophils and foamy macrophages (fm); bulla mucosa (m). (H) Higher magnification of image (G) shows the granuloma has an epithelial margin (e), embedded foreign body (fb) and capillaries (c). Macrophages in the granuloma and foamy macrophages (fm) in bulla exudate give stain positively for F4/80. (I) A granuloma located in the caudal bulla of a 14-week-old *Eda*^{Ta} mouse has PAS positive (plant-based) foreign body particle (fb) at the margin. (J) Hair shaft fragments (fb) in the neutrophil rich exudate (ex) of a 43-week-old *Eda*^{Ta} mouse; note plasma cell (pc) infiltration of the thickened bulla mucosa (m). Scale bars: 500 μm (A, C); 50 μm (B, D); 100 μm (E, F, H, J), 200 μm (G) 250 μm (I)

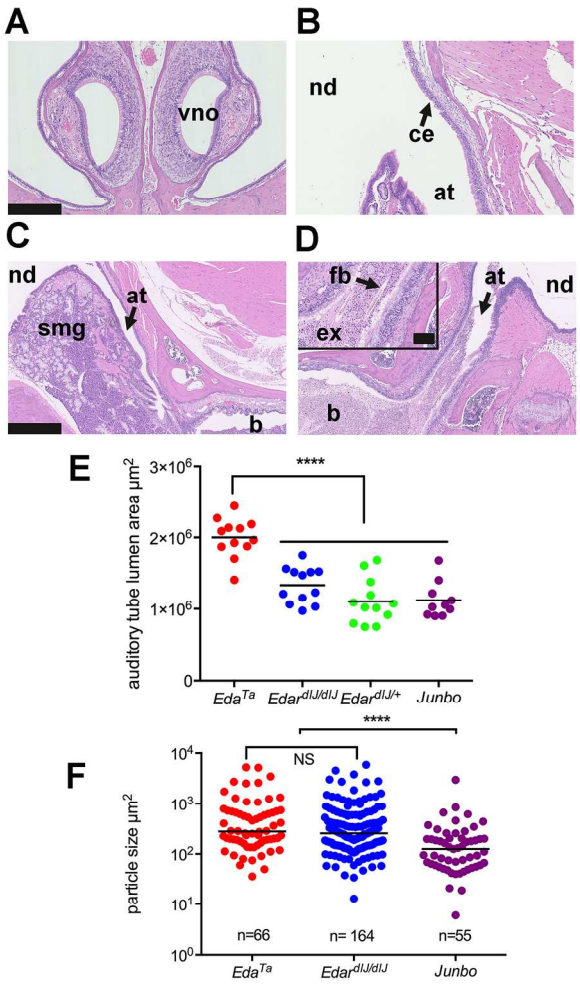

Figure 5. Auditory tube gating function is compromised in the absence of submucosal glands. (A) Coronal section of the rostral nose in a *Junbo* mouse has normal air filled nasal passages; note vomeronasal organ (vno). (B-D) Dorsal plane sections. (B) The opening of the auditory tube (at) into the nasopharynx (nd) in a *Junbo* mouse shows the normal mucosa of the nasopharynx is lined by ciliated epithelium (ce). (C, D) Nasopharynx (nd), auditory tubes (at) and bullae (b). (C) An auditory tube in a 45-week-old *Junbo* mouse with a slender profile and empty lumen; note submucosal glands (smg). (D) The auditory tube of a 13-week-old Eda^{Ta} mouse contains exudate (ex) and hair shaft foreign body material (fb) (inset shows higher magnification of the tube contents). (E) Auditory tube lumen area is significantly greater in Eda^{Ta} (n=6 mice, 13-weeks-old) than in $Edar^{dlJ/dlJ}$ (n=6 mice, 16-weeks-old), $Edar^{dlJ/+}$ (n=6 mice, 15-16 weeks-old) and *Junbo* (n=5 mice, 24-45 weeks-old). Total area for each auditory tube was measured in 50 µm step sections, and data are represented as points with the average as a bar; one-way ANOVA and Tukey's multiple comparison test; **** $P<0.0001$. (F) Bulla foreign body particle size in $Edar^{dlJ/dlJ}$ and Eda^{Ta} mice is significantly larger than in *Junbo* mice. Particle sizes were measured in the bullae of $Edar^{dlJ/dlJ}$ (n=11 mice, 7-17 weeks old), Eda^{Ta} (n=10, 13-30 weeks old) and *Junbo* (n=9, 14-45 weeks old) mice. The graph represents data points and the median as a bar; 2-tailed Kruskal Wallis test; ****$P<0.0001$ and NS not significant in Dunn's multiple comparison test. Scale bars: 250 µm (A, B); 500 µm (C, D); 100 µm (panel D inset).
180x199mm (300 x 300 DPI)

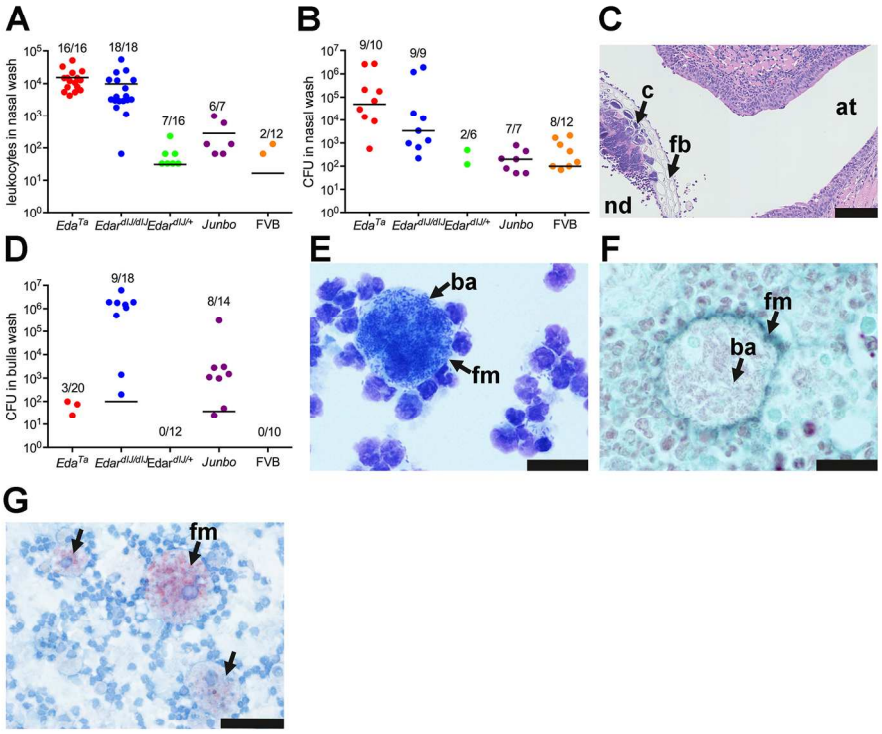

Figure 6. Commensal bacteria populations and inflammatory response in the nose and auditory bulla of EDA pathway deleted mice. (A) Leukocyte numbers in the nasal wash of *Edar*$^{dlJ/dlJ}$ and *Eda*^{Ta} mice are significantly elevated (see text for details) compared to FVB, *Edar*$^{dlJ/+}$ and *Junbo* mice. (B) Total bacterial load (CFU) in nasal samples are significantly elevated (see text for details) in *Edar*$^{dlJ/dlJ}$ (predominately *E. coli*) and *Eda*^{Ta} (predominately *Staphylococcus aureus*) mice than FVB, *Edar*$^{dlJ/+}$ and *Junbo* mice. (C) Cocci colonies (c) associated with plant foreign body (fb) in the nasopharynx (nd) at the opening of the auditory tube (at) of a 43-week-old *Eda*^{Ta} mouse. (D) Total bacterial load in bulla samples was highest in *Edar*$^{dlJ/dlJ}$ (predominately *E. coli*) and *Junbo* (mixed bacterial isolates, see Table S1 for bacterial isolate list). (E) Giemsa stained cytology of bulla exudate from an *E. coli* culture positive 11-week-old *Edar*$^{dlJ/dlJ}$ mouse shows a foamy macrophage with bacilli (ba); (F) a histology section shows the Gram-negative bacilli (ba) are intracytoplasmic; F4/80 IHC (Vector SG detection kit has a blue-grey chromogen) and Neutral Red counterstain. (G) Bulla foamy macrophages from a 13-week-old *Eda*^{Ta} mouse contain lipid bodies; formalin fixed cytology preparation stained with Oil Red O. (A, B, D) The graphs represent data points, the median (that incudes zero values) as a bar, and the ratio above each represents the number of positive samples divided by the total number sampled. Scale bars: 100 µm (C); 20 µm (E, F); 50 µm (G).
180x199mm (300 x 300 DPI)

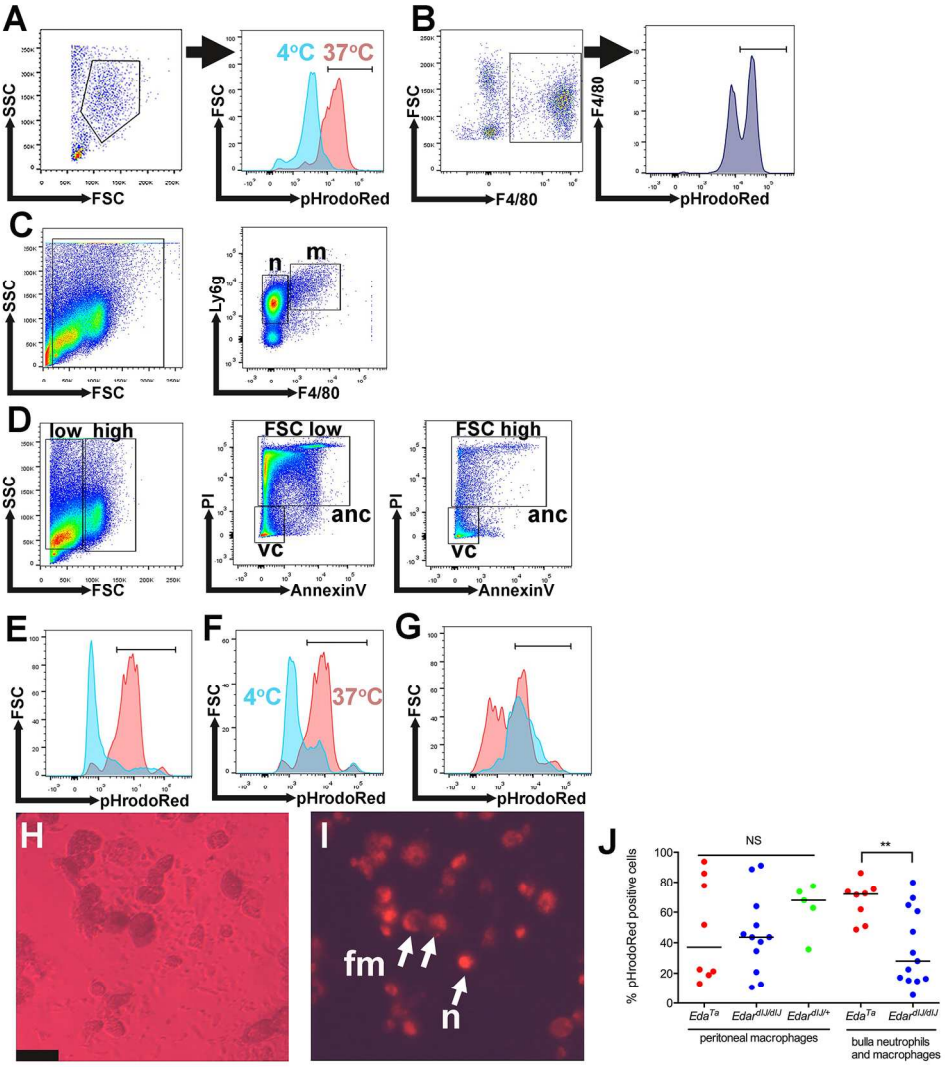

Figure 7. Immune cell populations and function in EDA pathway deleted mice. (A, B) Peritoneal macrophages. (A) A Forward Scatter (FSC) Side Scatter (SCS) plot shows the selected peritoneal macrophage population from an *Edar*$^{dlJ/+}$ mouse. The overlay histogram shows pHrodoRed fluorescence in the macrophage gate for a control sample incubated at 4°C to inhibit phagocytosis (blue) and sample incubated at 37°C (red). (B) FSC^{High} F4/80^{High} gated peritoneal macrophages analyzed for pHrodoRed fluorescent signals. (C-G) Bulla fluid leukocytes from *Edar*$^{dlJ/dlJ}$ mice. (C) FSC SSC selected leukocytes were analysed in a F4/80 Ly6g plot and 85.6% of the leukocytes were Ly6g^{High} F4/80^{Low} neutrophils (n) (median 95% CI 71.7-94.6%) and 2.1% were Ly6g^{High} F4/80^{High} macrophages (m) (95% CI, 1.2-3.5%). (D) FSC SSC plots were used to select two leukocyte populations. The FSC^{Low} SSC^{Low} gated leukocytes had 23.9% PI^{-} AnnexinV^{-} viable cells (v) (median 95% CI 11.1-52.3) and 74% PI^{+}AnnexinV^{+} apoptotic or necrotic cells (anc) (95% CI 41.6-76.3%). The FSC^{High} SSC^{High} gated leukocytes had 86.1% PI^{-} AnnexinV^{-} viable cells (median, 95% CI, 84.0-97.0) and 11.6% PI^{+}AnnexinV^{+} apoptotic or necrotic cells (95% CI 1.8-11.9%). (E-G) The overlay histograms for pHrodoRed fluorescence. (E) FSC^{Low} SSC^{Low} selected leukocytes (blue) have a low population of viable cells capable of phagocytosis, whereas FSC^{High} SSC^{High} selected leukocytes (red) have high population of viable cells capable of phagocytosis. (F) A FSC^{High} SSC^{High} selected PI^{-} AnnexinV^{-} viable leukocytes incubated at 37°C show a phagocytosis signal (red) but incubation at 4°C (blue) inhibits phagocytosis. (G) 56% of Ly6g^{High}F4/80^{Low} neutrophils (95% CI 50-71%) (red) were phagocytically active

and 72% of Ly6g^{High}F4/80^{High} macrophages (95% CI, 59-93%) (blue) were phagocytically active. (H, I) *Eda*^{Ta} mouse bulla leukocytes; (H) phase contrast image of cells; (I) pHrodoRed fluorescent image of the same field of view, the smaller cells are the same size as neutrophils (n), and larger cells are macrophages and foamy macrophages (fm). The untreated control had no detectable autofluorescent signal. Scale bar 50 µm. (J) The percentage of pHrodoRed positive peritoneal macrophages was not significantly different in *Eda*^{Ta}, *Edar*$^{dlJ/dlJ}$, *Edar*$^{dlJ/+}$ mice (Kruskal Wallis test); whereas the percentage of positive bulla neutrophils and macrophages was significantly higher in *Eda*^{Ta} than *Edar*$^{dlJ/dlJ}$ mice. The graph represents data points and the median as a bar. NS $P>0.05$; $^{**}P<0.01$.
180x199mm (300 x 300 DPI)

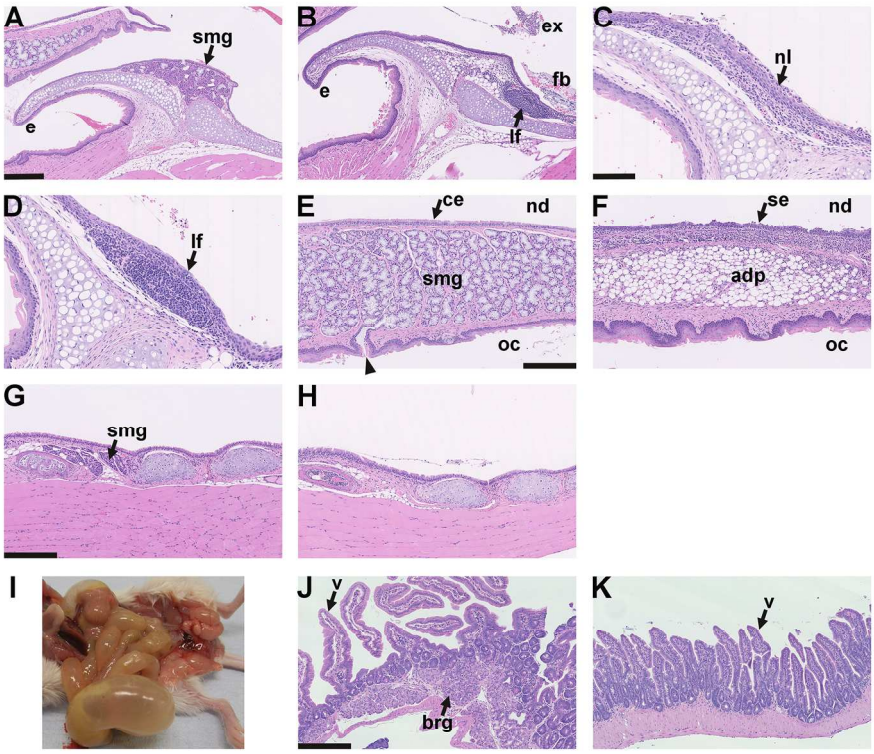

Figure 8. Larynx histology and aerophagia in EDA pathway deleted mice. A-D larynx mid-sagittal plane. (A) The epiglottis (e) of a 24-week-old FVB mouse has submucosal glands (smg) but these are absent in *Edar*$^{dlJ/dlJ}$ and *Eda*^{Ta} mice; (B) the epiglottis of 14-week-old *Edar*$^{dlJ/dlJ}$ mouse lacks glands and has a submucosal lymphoid follicle (lf); there is exudate (ex) and foreign body (fb) in the proximal trachea. (C, D) Two 25-week-old mice *Eda*^{Ta} mice; (C) one *Eda*^{Ta} mouse has neutrophil (nl) infiltration of the epiglottis epithelium, and (D) a higher magnification image of a submucosal lymphoid follicle (lf) in a second *Eda*^{Ta} mouse. (E, F) soft palate mid-sagittal plane. (E) The soft palate of a 24-week-old FVB mouse has submucosal gland comprising mucous cells (smg) that empty via ducts (arrow head) into the oral cavity (oc); nasopharynx (nd) is lined by ciliated epithelium (ce). (F) The soft palate of a 14-week-old *Edar*$^{dlJ/dlJ}$ mouse lacks submucosal glands and this region is occupied by adipose tissue (adp); the nasopharynx is lined by squamous epithelium (se). (G, H) trachea mid-sagittal plane. (G) The proximal trachea of a 14-week-old *Edar*$^{dlJ/+}$ mouse has submucosal glands (smg); (H) these glands are absent in a 25-week-old *Eda*^{Ta} mouse. (I) Post mortem appearance of an 18-week-old *Eda*^{Ta} mouse with aerophagia that has an air filled stomach, small intestines and caecum. (J, K) small intestine. (J) Duodenum of this *Eda*^{Ta} mouse has a normal submucosal Brunner's gland (brg) and villi (v); (K) the jejunum has an empty lumen. Scale bars: 250 μm (A, B, E-H, J, K); 100 μm (C, D).
180x199mm (300 x 300 DPI)